The Very Large Telescope Ultraviolet and Visible Echelle Spectrograph survey for molecular hydrogen in high-redshift damped Lyman α systems

Cédric Ledoux,[1]⋆ Patrick Petitjean[2,3]⋆ and R. Srianand[4]⋆

[1]*European Southern Observatory, Alonso de Córdova 3107, Casilla 19001, Vitacura, Santiago, Chile*
[2]*Institut d'Astrophysique de Paris – CNRS, 98bis Boulevard Arago, 75014, Paris, France*
[3]*LERMA, Observatoire de Paris, 61 Avenue de l'Observatoire, 75014, Paris, France*
[4]*IUCAA, Post Bag 4, Ganesh Khind, Pune 411 007, India*

ABSTRACT

We have searched for molecular hydrogen in damped Lyman α (DLA) and sub-DLA systems at high redshift ($z_{abs} > 1.8$) using the Ultraviolet and Visible Echelle Spectrograph (UVES) at the Very Large Telescope (VLT) down to a detection limit of typically $N(H_2) = 2 \times 10^{14}$ cm^{-2}. Out of the 33 systems in our sample, eight have firm and two have tentative detections of associated H_2 absorption lines. Considering that three detections were already known from past searches, molecular hydrogen is detected in 13–20 per cent of the newly surveyed systems. We report new detections of molecular hydrogen at $z_{abs} = 2.087$ and 2.595 toward, respectively, Q 1444+014 and Q 0405−443, and also reanalyse the system at $z_{abs} = 3.025$ toward Q 0347–383.

In all of the systems, we measure metallicities relative to solar, [X/H] (with either X = Zn, S or Si), and depletion factors of Fe, [X/Fe], supposedly on to dust grains, and compare the characteristics of our sample with those of the global population of DLA systems (60 systems in total). We find that there is a correlation between the metallicity and the depletion factor in both our sample and also the global population of DLA systems. Although H_2 molecules are detected in systems with [Zn/Fe] as small as 0.3, the DLA and sub-DLA systems where H_2 is detected are usually amongst those having the highest metallicities and the largest depletion factors. In particular, H_2 is detected in the five systems having the largest depletion factors. Moreover, the individual components where H_2 is detected have depletion factors systematically larger than other components in the profiles. In two different systems, one of the H_2-detected components even has [Zn/Fe]$\geqslant$1.4. These are the largest depletion factors ever seen in DLA systems. All of this clearly demonstrates the presence of dust in a large fraction of the DLA systems.

The mean H_2 molecular fraction, $f = 2N(H_2)/[2N(H_2) + N(H\,\textsc{i})]$, is generally small in DLA systems (typically log $f < -1$) and similar to what is observed in the Magellanic Clouds. There is no correlation between the observed amount of H_2 and the H\,\textsc{i} column density. In fact, two systems where H_2 is detected have log $N(H\,\textsc{i}) < 20.3$ and, therefore, are sub-DLA systems. From 58 to 75 per cent of the DLA systems have log $f < -6$. This can be explained if the formation rate of H_2 on to dust grains is reduced in those systems, probably because the gas is warm ($T > 1000$ K) and/or the ionizing flux is enhanced relative to what is observed in our Galaxy.

Key words: galaxies: ISM – quasars: absorption lines – quasars: individual: Q 0347−383 – quasars: individual: Q 0405−443 – quasars: individual: Q 1444+014 – cosmology: observations.

⋆E-mail: cledoux@eso.org (CL); petitjean@iap.fr (PP); anand @iucaa.ernet.in (RS)

1 INTRODUCTION

High-redshift damped Lyman α (DLA) systems observed in absorption against quasi-stellar object (QSO) spectra are characterized by their extremely strong H I $\lambda1215$ lines corresponding to large neutral hydrogen column densities, $N(\text{H I}) \geqslant 2 \times 10^{20}$ cm^{-2}. Hydrodynamical simulations suggest that DLA systems are located inside regions of overdensities of the order of 1000 and higher (see, e.g., Haehnelt, Steinmetz & Rauch 2000; Gardner et al. 2001) and that DLA systems at $z_{\text{abs}} \gtrsim 2$ occur very close (within 10–15 kpc) to the centre of L* galaxies. This is purely speculative, however, and the exact nature of DLA systems is still to be clarified. Though observational studies of DLA systems have been pursued over two decades now, important questions are still unanswered, such as: (i) the presence of *in situ* star formation activity in DLA systems, (ii) the connection between observed abundance ratios and dust content and (iii) how severe is the bias due to dust obscuration in current DLA samples. Assessing the molecular content of DLA systems can provide a direct handle on at least some of these issues.

Formation of H$_2$ is expected on the surface of dust grains if the gas is cool, dense and mostly neutral, and from the formation of negative hydrogen if the gas is warm and dust-free (see, e.g., Jenkins & Peimbert 1997; Cazaux & Tielens 2002). As the former process is most likely to be dominant in the neutral gas associated with DLA systems, it is possible to obtain an indirect indication of the amount of dust in DLA systems without depending on extinction and/or heavy element dust depletion effects. Moreover, from determining the populations of different rotational levels of H$_2$, one can constrain kinetic and rotational excitation temperatures as well as particle densities. The effective photodissociation of H$_2$ takes place in the energy range 11.1–13.6 eV through Lyman- and Werner-band absorption lines and, therefore, the intensity of the local ultraviolet (UV) radiation field can be derived from the observed molecular fraction. A direct determination of the local UV radiation field could have important implications in bridging the link between DLA systems and star formation activity in high-redshift galaxies.

At H I column densities as large as those measured in DLA systems, H$_2$ molecules are conspicuous in our Galaxy: gas clouds with $\log N(\text{H I}) > 21$ usually have $\log N(\text{H}_2) > 19$ (see, e.g., Savage et al. 1977; Jenkins & Shaya 1979). Given this fact, it is somewhat surprising that earlier searches for molecular hydrogen in DLA systems, though not systematic, have found either small values or upper limits on the molecular fraction of the gas, $f = 2N(\text{H}_2)/[2N(\text{H}_2) + N(\text{H I})]$ (Black, Chaffee & Foltz 1987; Levshakov et al. 1992). For a long time, only the DLA system at $z_{\text{abs}} = 2.811$ toward Q 0528–250 was known to contain molecular hydrogen (Levshakov & Varshalovich 1985; Foltz, Chaffee & Black 1988). More recently, Ge & Bechtold (1999) searched for H$_2$ molecules in a sample of eight DLA systems using the MMT moderate-resolution spectrograph (FWHM = 1 Å). Apart from the detection of molecular hydrogen at $z_{\text{abs}} = 1.973$ and 2.338 toward, respectively, Q 0013–004 and Q 1232+082 (Ge & Bechtold 1997; Ge, Bechtold & Kulkarni 2001), they measured in the other systems upper limits on f in the range 10^{-6}–10^{-4}.

The molecular hydrogen content of the above three systems, where H$_2$ was detected at intermediate spectral resolution, has been re-examined systematically using high spectral resolution data (FWHM = 0.1 Å), leading to $N(\text{H}_2) \sim 6 \times 10^{16}$ cm^{-2} and $f \sim 5 \times 10^{-5}$ toward Q 0528–250 (Srianand & Petitjean 1998), $5 \times 10^{17} < N(\text{H}_2) < 10^{20}$ cm^{-2} and $2 \times 10^{-3} < f < 0.2$ toward Q 0013–004 (Petitjean, Srianand & Ledoux 2002) and $N(\text{H}_2) \geqslant 2 \times 10^{17}$ cm^{-2} and $f \geqslant 4 \times 10^{-4}$ toward Q 1232+082

(Srianand, Petitjean & Ledoux 2000). Recent new detections are from Levshakov et al. (2002) at $z_{\text{abs}} = 3.025$ toward Q 0347–383 and Ledoux, Srianand & Petitjean (2002b) at $z_{\text{abs}} = 1.962$ toward Q 0551–366. Two tentative detections have also been reported at $z_{\text{abs}} = 2.374$ toward Q 0841+129 (Petitjean, Srianand & Ledoux 2000) and at $z_{\text{abs}} = 3.390$ toward Q 0000–263 (Levshakov et al. 2000) based, however, on the identification of two weak features located in the Lyman α forest.

This paper describes the high spectral resolution survey of high-redshift DLA systems, focused on the search for molecular hydrogen, that we have carried out at the European Southern Observatory (ESO) Very Large Telescope (VLT) during the first 2 years of operations of the Ultraviolet and Visible Echelle Spectrograph (UVES). We present here our final results from the observations of a total sample of 24 DLA [$\log N(\text{H I}) \geqslant 20.3$] and nine sub-DLA [$19.4 < \log N(\text{H I}) < 20.3$] systems, including two new H$_2$ detections. Preliminary results from the observations of a sample of 11 systems were presented in Petitjean et al. (2000). Section 2 in the present paper describes the observations, the data and the absorber sample, Section 3 gives details on three DLA/sub-DLA systems where H$_2$ is detected, and in both Sections 4 and 5 general results are discussed from the study of the whole sample. We give our conclusions in Section 6.

2 OBSERVATIONS AND SAMPLE

The Ultraviolet and Visible Echelle Spectrograph (Dekker et al. 2000), installed at the ESO VLT 8.2-m telescope, unit Kueyen, on Mount Paranal in Chile, was used during five visitor-mode runs, from 2000 April to 2002 January. During each run, we surveyed DLA and sub-DLA systems with the aim of searching for H$_2$ lines with redshifts in the range 1.8–3.4. In a first step, we observed the ($V < 19$) background QSOs twice for 1–1.5 h over wavelength ranges covering the location of the main metal lines of the absorption systems and possibly associated H$_2$ features in, respectively, the red and the blue arms of UVES (which were used simultaneously). For most of the targets, this resulted in a signal-to-noise ratio in excess of 10 in the blue. The quick-look data reduction package available at the telescope was extensively used to decide in real time whether H$_2$ absorption lines were present or not. This allowed us to optimize our observing strategy: in the case of detection, additional exposures were gathered to achieve the high signal-to-noise ratio needed for an accurate determination of the H$_2$ column densities in different rotational levels. In addition to our observations, we also included the few UVES archival spectra of QSOs with DLA systems for which the H$_2$ wavelength ranges were covered.

The total QSO sample presently under consideration is made of 25 lines of sight. Observations toward Q 0013−004, Q 0551−366 and Q 1232+082, along the lines of sight of which H$_2$ is detected, are described, respectively, in Petitjean et al. (2002), Ledoux et al. (2002b) and Srianand et al. (2000). In addition, new data for Q 0528−250 and Q 1232+082 were acquired recently and the corresponding H$_2$-detected systems should be analysed in detail in forthcoming papers. However, we give in Section 4 the measurement from UVES data of the molecular hydrogen and metal contents of the DLA system at $z_{\text{abs}} = 2.811$ toward Q 0528−250.

With respect to the remaining and/or new detections of H$_2$ in our sample, high-resolution, high signal-to-noise ratio spectra of Q 0347−383 ($z_{\text{em}} = 3.21$, $m_V = 17.8$), Q 0405−443 ($z_{\text{em}} = 3.02$, $m_B = 17.6$) and Q 1444+014 ($z_{\text{em}} = 2.21$, $m_{B_J} = 18.5$) were obtained on, respectively, 2002 January 7–9, 2001 October 20–23 and June 16. During the observations of Q 0405−443, central wavelengths

3900 and 5700 Å were used in, respectively, the blue and the red arms of UVES with dichroic no 1, and central wavelengths were adjusted to 4370 Å in the blue and 7400 Å in the red with dichroic no 2. Full wavelength coverage was achieved this way from 3283 to 7320 Å and from 7468 to 9302 Å, accounting for the gap between the two red-arm CCDs. During the observations of Q 1444+014 (respectively, Q 0347−383), central wavelengths were adjusted to 3800 Å (respectively, 4300 Å) in the blue and 5640 Å (respectively, 8000 Å) in the red, and we used dichroic no 1 (respectively, no 2). Complementary UVES data for Q 1444+014, obtained on 2000 May 29–30, with similar settings, were retrieved from the UVES archive. For each of the 25 quasars in our sample, the CCD pixels were binned 2×2 in both arms and the slit width was fixed to 1 arcsec (except for Q 0347−383: 0.8 arcsec) yielding a spectral resolution $R = 42\,500$ (respectively, $R = 52\,000$). The total integration times were 9×4500 s for Q 0347−383, 4×4350 s with dichroic no 1 (and 2×4350 s with dichroic no 2) for Q 0405−443, and 8×3600 s for Q 1444+014.

The spectra of each QSO were reduced in the dedicated context of MIDAS, the ESO data reduction system, using the UVES pipeline (Ballester et al. 2000) in an interactive mode. The main characteristics of the pipeline are to perform a precise interorder background subtraction for science frames and master flat-fields, and an optimal extraction of the object signal rejecting cosmic ray impacts and subtracting the sky spectrum simultaneously. The pipeline products were checked step by step. The wavelength scale of the spectra reduced by the pipeline was then converted to vacuum-heliocentric values and individual one-dimensional exposures were scaled, weighted and combined altogether using the SCOMBINE task of the NOAO ONEDSPEC package of IRAF. During this process, the spectra of each QSO were rebinned to a common wavelength step (0.05 Å pixel^{-1} or less). In particular, the spectra of Q 0347−383, Q 0405−443 and Q 1444+014, where H₂ is detected, were rebinned to, respectively, 0.03, 0.0471 and 0.0339 Å pixel^{-1}, yielding after combination of individual exposures signal-to-noise ratios in, respectively, the ranges 20–50, 10–50 and 10–45 in the blue and 90–15, 120–20 and 90–30 in the red.

Standard Voigt-profile fitting techniques were used to determine column densities, in all the absorption-line systems for which the H₂ wavelength range was observed, using the oscillator strengths compiled in Table 1 for metal ions and the oscillator strengths given by Morton & Dinerstein (1976) for H₂. In the following, we measure metallicities relative to solar, $[\mathrm{X/H}] \equiv \log[N(\mathrm{X})/N(\mathrm{H})] - \log[N(\mathrm{X})/N(\mathrm{H})]_\odot$, with either X = Zn, S or Si, and depletion factors of iron, $[\mathrm{X/Fe}] \equiv \log[N(\mathrm{X})/N(\mathrm{Fe})] - \log[N(\mathrm{X})/N(\mathrm{Fe})]_\odot$, adopting the solar abundances from Savage & Sembach (1996).

There has been no a priori selection of the systems. In our sample, the 24 DLA and nine sub-DLA absorbers are generally drawn at random from the global population of known systems. However, we have reobserved with UVES three DLA systems where H₂

Table 1. Atomic data.

Transition	λ_{vac} (Å)	f	Ref.[2]	Transition	λ_{vac} (Å)	f	Ref.[2]
H I λ1025	1025.7223	0.07912	a	Si II λ1808	1808.0129	0.00208	f
H I λ1215	1215.6701	0.4164	a	P II λ963	963.801	1.458	a
C I λ1328	1328.8333	0.0630	b	P II λ1152	1152.8180	0.236	a
C I *λ1329.08	1329.0853	0.0213	b	S II λ1250	1250.584	0.00545	a
C I *λ1329.10	1329.1004	0.0260	b	S II λ1253	1253.811	0.0109	a
C I *λ1329.12	1329.1233	0.0160	b	S II λ1259	1259.519	0.0162	a
C I λ1560	1560.3092	0.0719	b	Ar I λ1048	1048.2199	0.257	g
C I *λ1560.6	1560.6822	0.0539	b	Ti II λ1910.6	1910.609	0.104	h
C I *λ1560.7	1560.7090	0.0180	b	Ti II λ1910.9	1910.938	0.098	h
C I λ1656	1656.9283	0.139	b	Cr II λ2056	2056.2569	0.105	i
C I *λ1656	1656.2672	0.0589	b	Cr II λ2062	2062.2361	0.0780	i
C I *λ1657.3	1657.3792	0.0356	b	Cr II λ2066	2066.1640	0.0515	i
C I *λ1657.9	1657.9068	0.0473	b	Fe II λ1096	1096.8769	0.0324	j
C I **λ1657	1657.0082	0.104	b	Fe II λ1121	1121.9749	0.0202	j
C II *λ1037	1037.0182	0.123	a	Fe II λ1125	1125.4478	0.0163	j
C II *λ1335.6	1335.6627	0.0128	a	Fe II λ1143	1143.2260	0.0177	j
C II *λ1335.7	1335.7077	0.115	a	Fe II λ1144	1144.9379	0.106	j
N I λ1134.1	1134.1653	0.0134	a	Fe II λ1608	1608.4509	0.0585	j
N I λ1134.4	1134.4149	0.0268	a	Fe II λ1611	1611.2005	0.00136	j
N I λ1134.9	1134.9803	0.0402	a	Fe II λ2249	2249.8768	0.00182	j
N I λ1200.2	1200.2233	0.0885	a	Fe II λ2260	2260.7805	0.00244	j
O I λ950	950.8846	0.00157	a	Fe II λ2374	2374.4612	0.0313	j
O I λ974	974.07(5)[1]	0.00002	a	Ni II λ1317	1317.2170	0.0774	k
Mg II λ1239	1239.9253	0.000554	c	Ni II λ1370	1370.1320	0.0765	k
Mg II λ1240	1240.3947	0.000277	c	Ni II λ1741	1741.5531	0.0427	l
Al II λ1670	1670.7886	1.833	a	Ni II λ1751	1751.9157	0.0277	l
Si II λ1020	1020.6989	0.0283	a	Zn II λ2026	2026.1371	0.489	i
Si II λ1304	1304.3702	0.0894	d	Zn II λ2062	2062.6604	0.256	i
Si II λ1526	1526.7070	0.127	e				

[1]See Subsection 3.1.

[2]References for oscillator strengths: (a) Morton (1991); (b) Wiese, Fuhr & Deters (1996); (c) Welty et al. (1999); (d) Spitzer & Fitzpatrick (1993); (e) Schectman, Povolny & Curtis (1998); (f) Bergeson & Lawler (1993b); (g) Federman et al. (1992); (h) Wiese, Fedchak & Lawler (2001); (i) Bergeson & Lawler (1993a); (j) Howk et al. (2000); (k) Fedchak & Lawler (1999); (l) Fedchak, Wiese & Lawler (2000).

was previously detected (toward Q 0013−004, Q 0528−250 and Q 1232+082). Finally, the number of lines of sight along which several systems are seen is larger in our sample than in the global population of DLA systems. One would expect this to introduce a bias in favour of low-metallicity absorbers. However, the characteristics of our sample and those of the global population of DLA systems are compared in Section 4 and they are shown to be similar.

3 DESCRIPTION OF INDIVIDUAL SYSTEMS WITH H₂ DETECTION

In this section, we reconsider the case of the DLA system at $z_{abs} = 3.025$ toward Q 0347−383 and describe two new detections of molecular hydrogen at, respectively, $z_{abs} = 2.595$ and 2.087 toward, respectively, Q 0405−443 and Q 1444+014.

3.1 Q 0347−383, $z_{abs} = 3.025$

The detection of molecular hydrogen toward this quasar has been reported recently by Levshakov et al. (2002) who used UVES commissioning data. As part of our systematic survey, we have obtained significantly better UVES data for this line of sight and we reanalyse here the DLA system at $z_{abs} = 3.025$ on the same footing as the rest of our sample.

We display in Fig. 1 the velocity profiles of the most important lines from low ions and neutral species that are present in our data. Two well-separated components are observed for a number of ions, namely N I, O I, Si II, P II, S II and Ar I. One of these two components, at $z_{abs} = 3.02485$, has detected H₂ lines.

Fitted altogether (see below), the detected H₂ lines are found to be consistently located at a redshift of 3.024 89 and show a systematic offset of ∼3 km s⁻¹ relative to the deepest part of the low-ion profiles. We simultaneously fitted the lines from different rotational levels using the same broadening parameter and redshift, and measured accurate column densities for the $J = 0–4$ levels from subsamples of four to seven unblended lines per J level. The results are given in Table 2 and the best-fitting model is shown in Fig. 2. Note, in particular, that the measurement of the column density in $J = 0$ is based on the detection at more than 5σ of four transition lines: W 1–0 R(0), L 7–0 R(0), L 3–0 R(0) and L 2–0 R(0). A 3σ absorption feature, possibly corresponding to C I λ1656, is also detected at a redshift consistent with that of the H₂ lines. If this is true then $\log N(\mathrm{C\,I}) = 11.73 \pm 0.26$ (see Table 3). The second low-ion line component, at $z_{abs} = 3.02463$, has no detected H₂ down to, respectively, $\log N(\mathrm{H_2}) < 13.0$ and <13.4 (5σ limits) for, respectively, $J = 0$ and 1. We measured in this DLA system a total neutral hydrogen column density $\log N(\mathrm{H\,I}) = 20.56 \pm 0.05$ (see Fig. 3) and a total molecular hydrogen column density $\log N(\mathrm{H_2}) = 14.55 \pm 0.09$ (see Table 2). This leads to an overall molecular fraction, $\log f = -5.71 \pm 0.10$, in agreement with that derived by Levshakov et al. (2002).

We measured ionic column densities in the two main components of the system and in two weaker ones only for species with unsaturated and/or mildly saturated lines. The results are given in Table 3. The broadening parameters were mainly constrained by Fe II and, to some extent also, N I lines covering a range of oscillator strengths. It can be seen in Fig. 1 that in our data the Zn II doublet lines are firmly detected in between sky lines in the strongest component of the system ($z_{abs} = 3.02485$) and are also likely to be present in the component at $z_{abs} = 3.024\,63$. In addition, the Cr II triplet is nicely detected in each of the four considered components (see Fig. 1 and Table 3).

In Fig. 1, we show evidence that the Si II λ1808 line is badly blended with a telluric absorption feature, which we have carefully removed via modelling. The best-fitting of the S II λ1259 line from the Keck-HIRES spectrum of Prochaska & Wolfe (1999, private communication) and of both Si II λλ1020,1808 lines in our VLT-UVES spectrum implies that the α-element to iron-peak elemental ratio derived from the two main components of the system is close to solar and may even be slightly undersolar: [S, Si/Zn] = −0.11 ± 0.09, − 0.35 ± 0.09. This is line with the findings of studies of large DLA samples (Ledoux, Bergeron & Petitjean 2002a; Prochaska & Wolfe 2002). In addition, we report the first detection of the O I λ974 line in a DLA system (at the 4σ significance level; see Fig. 1). The vacuum wavelength and the oscillator strength of this line are poorly known quantities, however (see Morton 1991). In order to fit the line, we used $\lambda_{vac} = 974.075$ Å, and we included at the end an extra 20 per cent uncertainty on the measured O I column density to reflect the uncertainty on the oscillator strength. We obtain [O/Zn] = 0.00 ± 0.20. Being solar, this ratio is in agreement with those previously derived for S and Si. This is at variance with the claim by Levshakov et al. (2002) that in this DLA system α-elements are strongly overabundant compared with zinc ([α/Zn] = 0.6 ± 0.1). The latter authors have underestimated both the contamination of metal lines by telluric absorption features at $\lambda_{obs} > 7000$ Å and also the saturation of O I lines in the Lyman α forest.

We compute metallicities [Zn/H] = −0.98 ± 0.09 and [S/H] = −1.09 ± 0.06, and a mean depletion factor [Zn/Fe] = 0.74 ± 0.09, using the integrated column densities from the two main components of the system at $z_{abs} = 3.02463$ and 3.024 85. Interestingly, the depletion, supposedly on to dust grains, and possibly also the metallicity, is larger in the component where H₂ is detected ([Zn, S/Fe] = 1.07 ± 0.06, 0.79 ± 0.06 at $z_{abs} = 3.02485$) relative to the other components ([Zn, S/Fe] = 0.47 ± 0.12, 0.54 ± 0.04 and [S/Fe] = 0.06 ± 0.12 at, respectively, $z_{abs} = 3.02463$ and 3.025 01). Fig. 1 indeed strikingly shows that the absorption-line profiles of little or non-depleted elements, such as Si, P and S, are different from, for example, the Cr and Fe profiles in their being approximately twice as narrow.

3.2 Q 0405−443, $z_{abs} = 2.595$

Lopez et al. (2001) reported the discovery of three DLA candidates in a low-resolution spectrum of Q 0405−443. We confirm here from UVES spectroscopy the damped nature of these absorption systems at redshifts $z_{abs} = 2.550$, 2.595 and 2.621. Because the continuum of this quasar is especially well defined in our high-resolution spectra, we are able to derive accurate total neutral hydrogen column densities for each absorber. For this, we fitted the Lyman series from Lyα to Ly6 and obtain $\log N(\mathrm{H\,I}) = 21.00 \pm 0.15$, 20.90 ± 0.10 and 20.25 ± 0.10 at, respectively, the above redshifts. Fig. 4 shows the best fit to the data, which is in practice mainly constrained by the combination of Lyα and Lyβ. An analysis of the three absorption systems is published in Lopez & Ellison (2003) who have independently acquired UVES data of a similar quality for the purpose of studying elemental abundances. We concentrate here on only some of the metal lines observed in the DLA system at $z_{abs} = 2.595$ (see Fig. 5) as in this particular absorber we found H₂.

Molecular hydrogen at $z_{abs} = 2.595$ is detected in the $J = 0$, 1, 2 and 3 rotational levels. Interestingly, quite a large number of H₂ lines from the $L = 0$ to 14 Lyman bands are observed at signal-to-noise ratios of the order of 10–30 from $\lambda_{obs} = 3500$ to 4000 Å. This leads to a precise determination of the molecular hydrogen
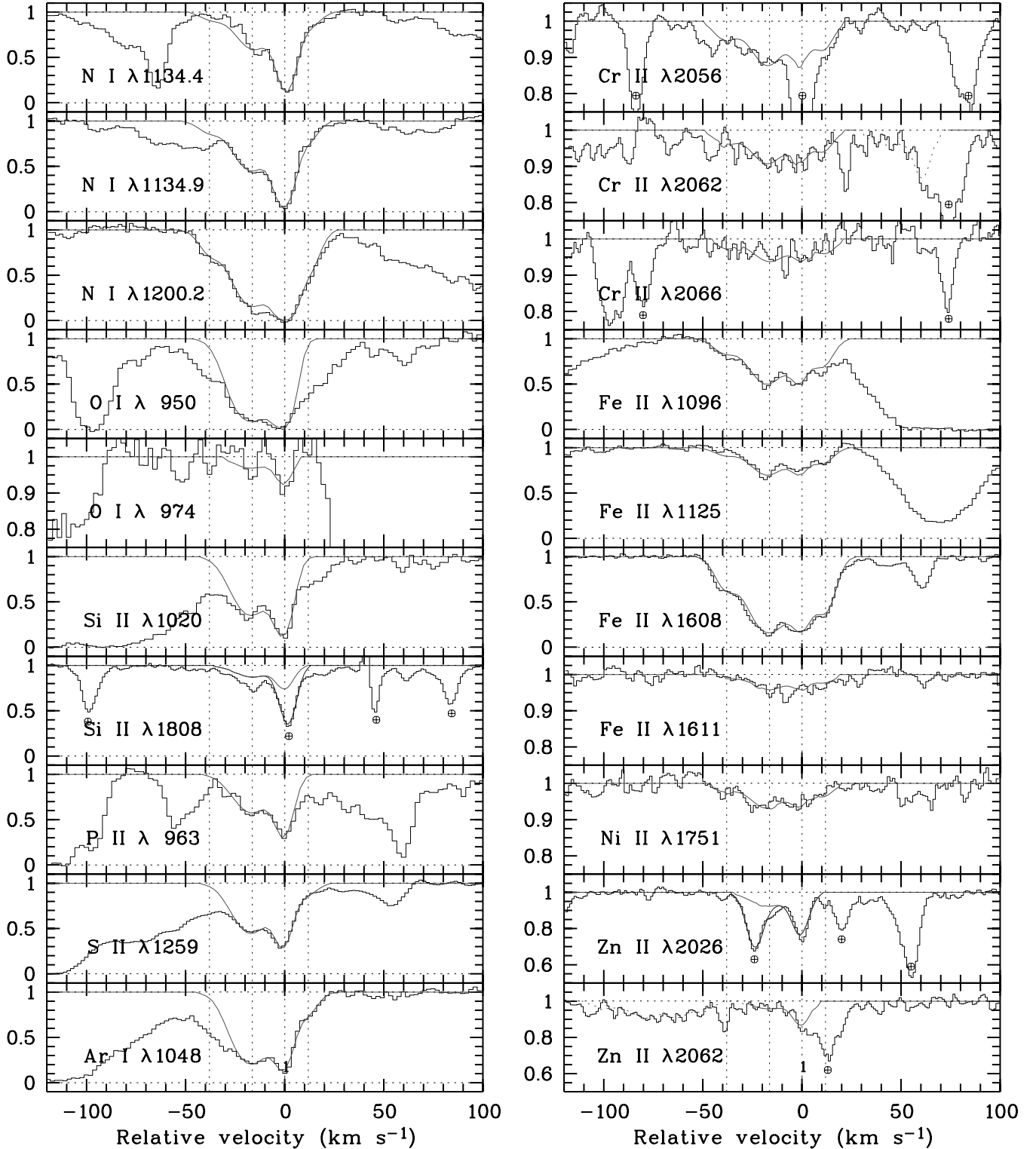
Figure 1. Velocity profiles of lines from low ions and neutral species in the DLA system at $z_{abs} = 3.025$ toward Q 0347−383. The S II λ1259 profile is reproduced from Prochaska & Wolfe (1999). Our best-fitting model is superimposed on the spectra with vertical lines marking the location of individual components. The dotted parts in some of the synthetic profiles correspond to other transitions than those indicated (Zn II λ2062 and Cr II λ2062). The single component where H₂ is detected is labelled with number 1. The location of telluric absorption features is marked by the symbol ⊕. Note that the blending with telluric lines has been carefully taken into account (dark curves) for the fitting of the Si II λ1808 and Zn II λ2026 profiles (light curves).

Table 2. Voigt-profile fitting results for different rotational levels of the vibrational ground-state Lyman and Werner bands of H_2 toward Q 0347−383.

z_{abs}	Level	$\log N \pm \sigma_{\log N}$ (H$_2$)	$b \pm \sigma_b$ (km s^{-1})
3.024 89	$J = 0$	13.25 ± 0.08	1.3 ± 0.2
	$J = 1$	14.26 ± 0.06	1.3 ± 0.2
	$J = 2$	13.65 ± 0.04	1.3 ± 0.2
	$J = 3$	13.90 ± 0.04	1.3 ± 0.2
	$J = 4$	13.12 ± 0.12	1.3 ± 0.2
	$J = 5$	$\leqslant 12.75^a$	1.3 ± 0.2

[a]Possible blends.

column densities in $J = 0$ and 1, and to some extent also in $J = 2$ and 3 (however, see below). Unsaturated and/or only moderately strong lines are observed for all $J \leqslant 3$ and damping wings are present in Werner-band lines from $J = 0$ and 1. We simultaneously fitted all unblended lines from different rotational levels, using the same broadening parameter and redshift, with a single component at $z_{abs} = 2.594\,71$. The column density in each J level was derived from several trials of Voigt-profile fitting to take into account the range of possible b values. Errors in the column densities therefore correspond to a range of column densities and not to the rms error from fitting the Voigt profiles. The results are given in Table 4 and the best-fitting model is shown in Fig. 6. The broadening parameter is found to be $b = 1.5$ km s^{-1}. We note, however, that the relative strengths of the $J \geqslant 2$ lines require $b \gtrsim 1.5$ km s^{-1}, whereas the $J \leqslant 1$ lines are consistent with $b \lesssim 1.5$ km s^{-1}. The broadening parameter could thus be smaller for lines from lower J and larger for lines from higher J, which may affect the determination of the column densities only in $J \geqslant 2$.

The total molecular hydrogen column density measured in this system, $\log N(H_2) = 18.16^{+0.21}_{-0.06}$, is one of the largest ever seen in DLA systems (see Section 4). However, the corresponding molecular fraction, $\log f = -2.44^{+0.23}_{-0.12}$, is relatively small due to the fairly large total neutral hydrogen column density. In spite of the high signal-to-noise ratio in our data at the location of the C I $\lambda1656$ transition line, neutral carbon is not clearly detected. A $\gtrsim 5\sigma$ absorption feature, the origin of which is uncertain, is present at $z_{abs} = 2.594\,85$, corresponding to $\log N(C\,I) \leqslant 11.95$.

We measured ionic column densities in the three main components of the system and in a weaker one. The results are given in Table 5. The component where H_2 is detected is not seen at all in Fe II, but is prominent in the C II * profile and detected in Si II, S II and Zn II (see Fig. 5). A careful modelling of the central blend leads to an accurate determination of the column densities of the latter ions, and to an upper limit on the column density of Fe II in the component at $z_{abs} = 2.594\,74$, which is probably associated with the
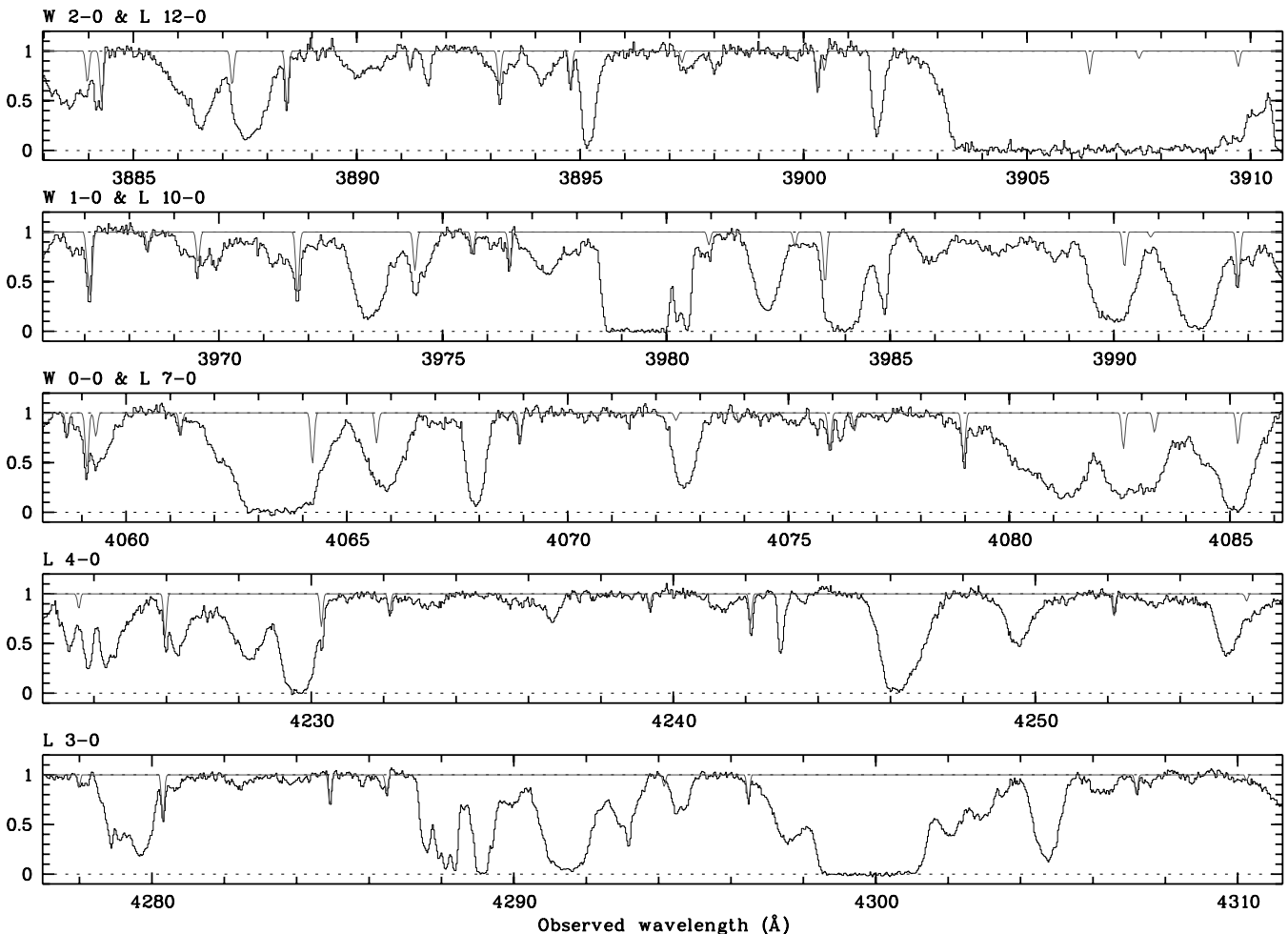

Figure 2. Voigt-profile fitting to the transition lines from the $J = 0, 1, 2, 3$ and 4 rotational levels of the vibrational ground-state Lyman and Werner bands of H_2 at $z_{abs} = 3.02489$ toward Q 0347−383. Only a few of the observed bands are displayed. H_2 is detected on this line of sight in a single gas cloud.

Table 3. Ionic column densities in individual components of the DLA system at $z_{abs} = 3.025$ toward Q 0347−383.

Ion	Transition lines used	$\log N \pm \sigma_{\log N}$	$b \pm \sigma_b$ (km s^{-1})
$z_{abs} = 3.024\,34$			
N I	1134.4,1134.9,1200.2	13.14 ± 0.08	06.7 ± 0.8
Cr II	2056,2062,2066	12.09 ± 0.14	06.7 ± 0.8
Fe II	1096,1125,1144[a]	13.36 ± 0.06	06.7 ± 0.8
Ni II	1741,1751	12.37 ± 0.36	06.7 ± 0.8
$z_{abs} = 3.024\,63$			
N I	1134.4,1134.9,1200.2	14.15 ± 0.03	11.4 ± 0.8
O I	950,974	16.12 ± 0.12[b]	11.4 ± 0.8
Si II	1020,1808	14.47 ± 0.03	11.4 ± 0.8
P II	963	12.34 ± 0.19[c]	11.4 ± 0.8
S II	1259[d]	14.50 ± 0.03	11.4 ± 0.8
Ar I	1048	13.68 ± 0.03	11.4 ± 0.8
Ti II	1910.6,1910.9	<11.86[e]	11.4 ± 0.8
Cr II	2056,2062,2066	12.69 ± 0.05	11.4 ± 0.8
Fe II	1096,1125,1144[a]	14.20 ± 0.02	11.4 ± 0.8
Ni II	1741,1751	13.07 ± 0.09	11.4 ± 0.8
Zn II	2026,2062	11.81 ± 0.12	11.4 ± 0.8
$z_{abs} = 3.024\,85$			
C I	1656[f]	11.73 ± 0.26	. . .
C I *	1656	<11.75[e]	. . .
C I **	1657	<11.50[e]	. . .
C II *	1037	13.55 ± 0.23	04.9 ± 0.3
N I	1134.4,1134.9,1200.2	14.47 ± 0.03	04.9 ± 0.3
O I	950,974	16.18 ± 0.18[b]	04.9 ± 0.3
Si II	1020,1808	14.48 ± 0.04	04.9 ± 0.3
P II	963	12.48 ± 0.09[c]	04.9 ± 0.3
S II	1259[d]	14.36 ± 0.04	04.9 ± 0.3
Ar I	1048	13.44 ± 0.05	04.9 ± 0.3
Ti II	1910.6,1910.9	<11.86[e]	04.9 ± 0.3
Cr II	2056,2062,2066	12.29 ± 0.11	04.9 ± 0.3
Fe II	1096,1125,1144[a]	13.81 ± 0.05	04.9 ± 0.3
Ni II	1741,1751	12.65 ± 0.19	04.9 ± 0.3
Zn II	2026,2062	12.02 ± 0.04	04.9 ± 0.3
$z_{abs} = 3.025\,01$			
N I	1134.4,1134.9,1200.2	13.44 ± 0.04	06.1 ± 0.5
S II	1259[d]	13.51 ± 0.12	06.1 ± 0.5
Ar I	1048	12.71 ± 0.06	06.1 ± 0.5
Cr II	2056,2062,2066	12.25 ± 0.09	06.1 ± 0.5
Fe II	1096,1125,1144[a]	13.69 ± 0.03	06.1 ± 0.5
Ni II	1741,1751	12.56 ± 0.17	06.1 ± 0.5

[a] Also 1608, 1611.

[b] An additional error of 20 per cent was incorporated to reflect the uncertainty on the oscillator strength of the O I λ974 line (see Morton 1991).

[c] The quoted error takes into account the main uncertainty which is related to the continuum placement because the single line used is located in a crowded Lyman α forest.

[d] Line observed by Prochaska & Wolfe (1999).

[e] 5σ upper limit.

[f] A 3σ absorption feature is detected at $z_{abs} = 3.024\,90$ (~3 km s^{-1} redward of $z_{abs} = 3.02485$), while the H$_2$ lines are consistently fitted with a single component at $z_{abs} = 3.02489$ (see Table 2).

H$_2$ absorption lines (see Table 5). We compute overall metallicities $[Zn/H] = -1.02 \pm 0.12$ and $[S/H] = -1.07 \pm 0.10$, and a mean depletion factor $[Zn/Fe] = 0.31 \pm 0.08$. As previously in the case of the DLA system toward Q 0347−383, the depletion is found to be larger in the component where H$_2$ is detected ($[Zn/Fe] > 0.70$ at $z_{abs} = 2.59474$) relative to the other components ($[Zn/Fe] = 0.38 \pm$
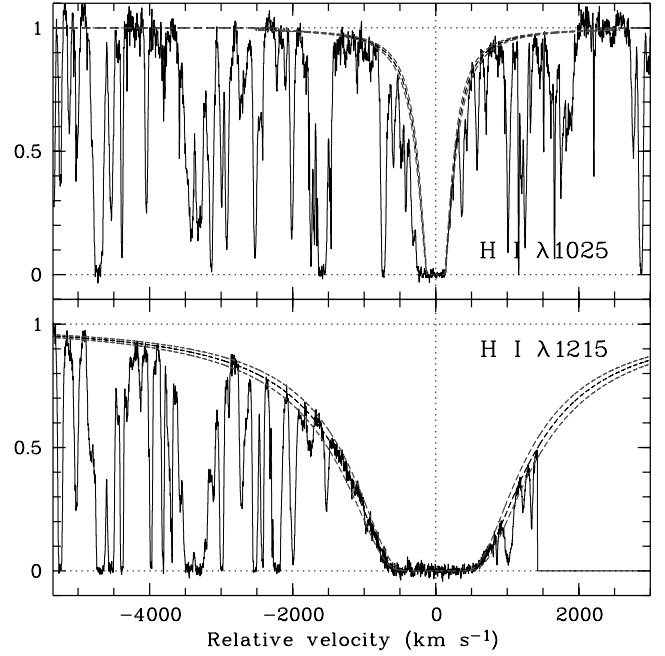
Figure 3. Portions of the normalized UVES spectrum showing the damped Lyα and Lyβ lines of the DLA system at $z_{abs} = 3.025$ toward 0347−383. The best-fitted Voigt profiles superimposed on the data correspond to $N(\mathrm{H\,I}) = (3.6 \pm 0.4) \times 10^{20}$ cm^{-2}.

0.11, 0.25 ± 0.06 and 0.28 ± 0.05 at, respectively, $z_{abs} = 2.59440$, 2.594 64 and 2.594 85).

3.3 Q 1444+014, $z_{abs} = 2.087$

Voigt-profile fitting to the Lyman α line of this absorption system leads to a total neutral hydrogen column density $\log N(\mathrm{H\,I}) = 20.07 \pm 0.07$ (see Fig. 7). Although this system would thus not qualify as a DLA system following the conventional definition, strong associated H$_2$ lines are detected. Moreover, Al III, Si IV and C IV lines are barely detected at $z_{abs} \approx 2.087$, which shows that the amount of highly ionized gas is small in the system. The overall metal line profiles are unusual in displaying a series of well-separated subsystems spread over ~400 km s^{-1}. However, the N I, P II and Zn II profiles suggest that most of the neutral hydrogen is concentrated within ~40 km s^{-1} of the central clump (see Fig. 8). This is confirmed by the detection of several C I lines from different excitation states in two components at $z_{abs} = 2.08685$ and 2.086 97 (velocity separation 12 km s^{-1}; see Fig. 9). The component at $z_{abs} = 2.086\,97$ is narrow and unresolved; the measured b-value is 1.1 km s^{-1} (see Table 6).

Molecular hydrogen lines from the $J = 0$, 1, 2 and 3 rotational levels are detected in two different components most clearly seen in $J \geqslant 2$ (see Fig. 10). Damping wings are definitively absent in $J = 0$ and 1. The redshifts of the H$_2$ components are consistent with those of the C I lines. Since the latter are accurately determined, we simultaneously fitted all unblended H$_2$ lines from different rotational levels with two components located at the measured redshifts of the C I lines. For a given component, the same broadening parameter was used independently of the J level of the lines. The column density in each J level was derived from several trials of Voigt-profile fitting to take into account the range of possible b values. Errors in the column densities therefore correspond to a range of column densities and not to the rms error from fitting the Voigt profiles. The results are given in Table 7.
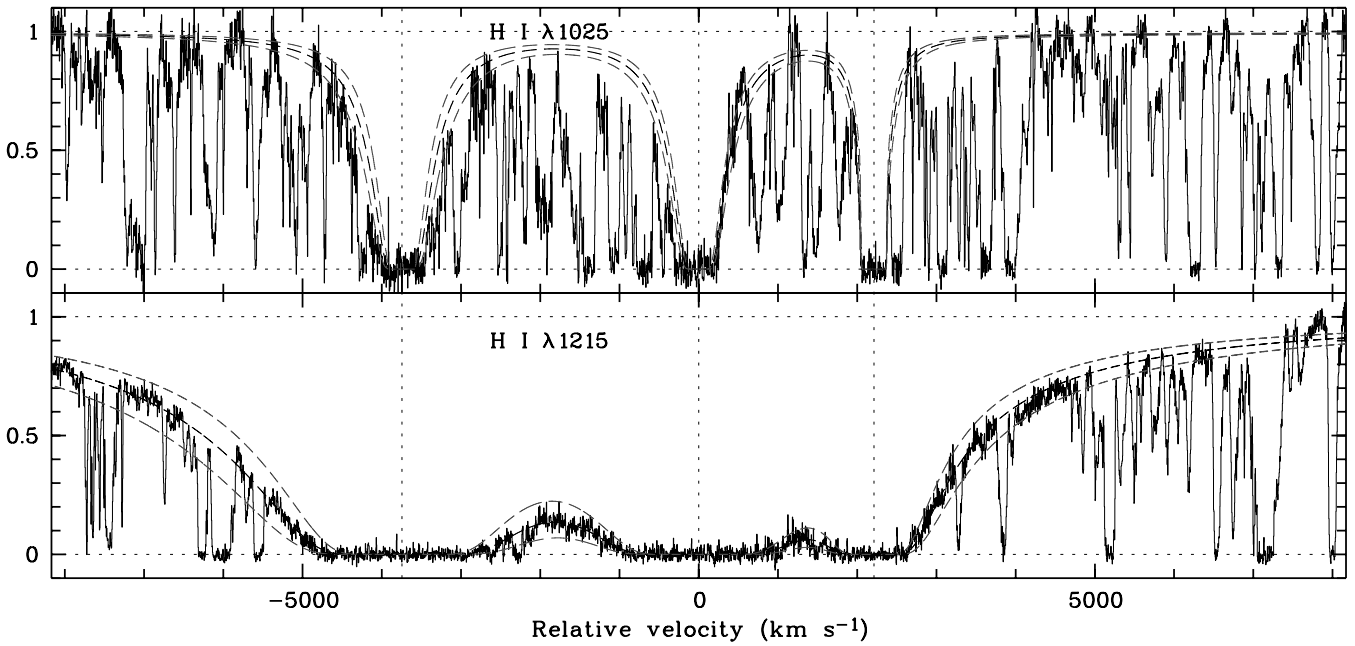
Figure 4. Portions of the normalized UVES spectrum showing the damped Lyα and Lyβ lines of the DLA/sub-DLA systems at z_{abs} = 2.550, 2.595 and 2.621 (see vertical lines) toward Q 0405−443. The best-fitted Voigt profiles superimposed on the data correspond to $N(H_I)$ = $(10 \pm 4, 7.9 \pm 2.1, 1.8 \pm 0.5) \times 10^{20}$ cm^{-2} for each of the systems, respectively.

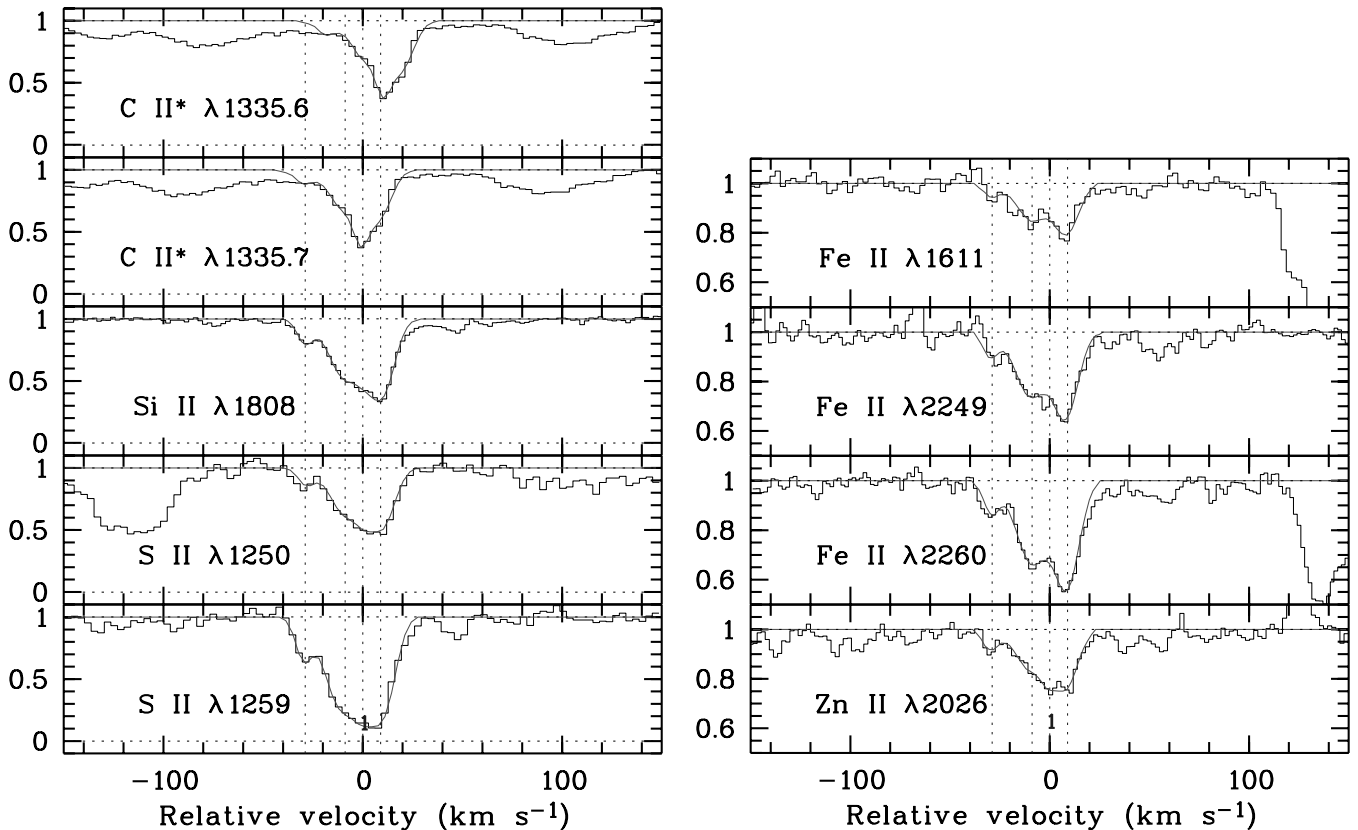**Figure 5.** Velocity profiles of some of the low-ion lines in the DLA system at z_{abs} = 2.595 toward Q 0405−443. Our best-fitting model is superimposed on the spectra with vertical lines marking the location of individual components. The single component where H_2 is detected is labelled with number 1. This component is clearly seen in the C II *λ1335.7 transition line and, to some extent also, in the S II and Zn II profiles.

Table 4. Voigt-profile fitting results for different rotational levels of the vibrational ground-state Lyman and Werner bands of H$_2$ toward Q 0405−443.

z_{abs}	Level	$\log N \pm \sigma_{\log N}$ (H$_2$)	$b \pm \sigma_b$ (km s^{-1})
2.594 71	$J = 0$	$17.73^{+0.15}_{-0.05}$	1.5 ± 0.5
	$J = 1$	$17.95^{+0.20}_{-0.05}$	1.5 ± 0.5
	$J = 2$	$15.71^{+0.90}_{-0.49}$	1.5 ± 0.5
	$J = 3$	$14.70^{+0.70}_{-0.22}$	1.5 ± 0.5
	$J = 4$	$<13.87^a$	1.5 ± 0.5
	$J = 5$	$<13.50^a$	1.5 ± 0.5

Note: errors in the column densities correspond to a range of column densities; they are not the rms errors from fitting the Voigt profiles (see the text).

[a] 5σ upper limit.

The line profiles of S II and Zn II on the one hand, and Si II and Fe II on the other hand, are different in the central clump (see Fig. 8). Whereas the S II and Zn II profiles have a rectangular shape with two main components, the redder of these two components is barely detected in the wing of the clump in both Si II λ1304 and Fe II λ1608. This demonstrates that Si and Fe depletions are much larger in the latter component. The redshifts of the main components of the system, in addition to a third one, were determined from simultaneous fitting of most of the observed metal lines but independently of the fitting to the C I lines. This shows an apparent velocity offset of ∼5 km s^{-1} between C I and other metal lines. The ionic column densities in the component in the red wing of the clump could also be derived accurately for a few species in the case of refractory elements using several transition lines covering a range of oscillator strengths (see Table 6). We find [Zn/Si] = 0.41 ± 0.13 and [Zn/Fe] = 0.69 ± 0.13 at z_{abs} = 2.086 79, and [Zn/Si] = 0.85 ± 0.09 and [Zn/Fe] = 1.40 ± 0.11 at z_{abs} = 2.086 92. This is reminiscent of warm and cold Galactic disc cloud dust-depletion patterns, respectively. The large depletion factors measured in the component at z_{abs} = 2.086 92 are of the same order of magnitude as those measured in the component at z_{abs} = 1.968 22 toward Q 0013−004 (Petitjean et al. 2002). This shows that, even though the depletion factors averaged over the entire profiles of DLA systems are usually moderate, they can be quite large in individual components.

4 THE H$_2$-SURVEY SAMPLE

In this section, we discuss all H$_2$ measurements performed to date at high spectral resolution in DLA and sub-DLA systems at high redshift ($z_{abs} > 1.8$). These measurements are summarized in Table 8. The H$_2$ and H I column densities are the total ones integrated over the systems, except for Q 0013−004 for which two subsystems could be studied individually. In most of the systems, there are several
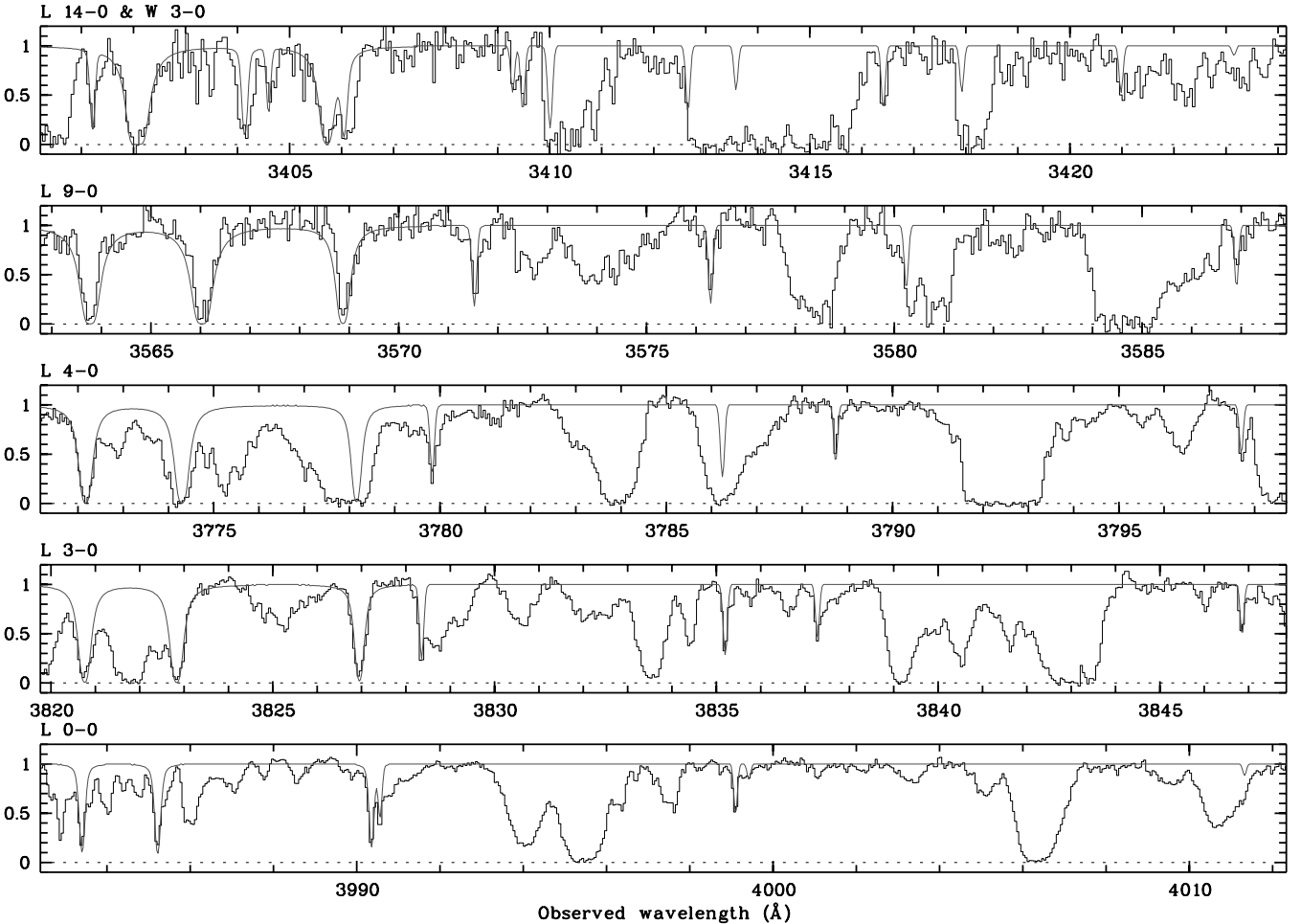

Figure 6. Voigt-profile fitting to the transition lines from the $J = 0$, 1, 2 and 3 rotational levels of the vibrational ground-state Lyman and Werner bands of H$_2$ at z_{abs} = 2.59471 toward Q 0405−443. Only a few of the observed bands are displayed. H$_2$ is detected on this line of sight in a single gas cloud.

Table 5. Ionic column densities in individual components of the DLA system at $z_{abs} = 2.595$ toward Q 0405−443.

Ion	Transition lines used	$\log N \pm \sigma_{\log N}$	$b \pm \sigma_b$ (km s^{-1})
$z_{abs} = 2.594\,40$			
C II *	1335.6,1335.7	$\leqslant 12.41 \pm 0.14$	3.7 ± 0.2
Si II	1808	14.35 ± 0.05	3.7 ± 0.2
S II	1250,1259	13.91 ± 0.04	3.7 ± 0.2
Fe II	2249,2260,2374[a]	13.98 ± 0.02	3.7 ± 0.2
Zn II	2026	11.50 ± 0.11	3.7 ± 0.2
$z_{abs} = 2.594\,64$			
C II *	1335.6,1335.7	13.09 ± 0.10	9.8 ± 0.2
Si II	1808	15.11 ± 0.02	9.8 ± 0.2
S II	1250,1259	14.72 ± 0.02	9.8 ± 0.2
Fe II	2249,2260,2374[a]	14.72 ± 0.04	9.8 ± 0.2
Zn II	2026	12.11 ± 0.04	9.8 ± 0.2
$z_{abs} = 2.594\,74$[b]			
C I	1656	<11.84[c]	...
C I *	1656	<11.95[c]	...
C I **	1657	<11.82[c]	...
C II *	1335.6,1335.7	13.20 ± 0.20	2.9:
Si II	1808	14.16 ± 0.14	2.9:
S II	1250,1259	14.07 ± 0.09	2.9:
Fe II	2249,2260,2374[a]	<13.68[d]	2.9:
Zn II	2026	11.52 ± 0.13	2.9:
$z_{abs} = 2.594\,85$			
C I	1656	$\leqslant 11.95 \pm 0.34$:	...
C I *	1656	<11.95[c]	...
C I **	1657	<11.82[c]	...
C II *	1335.6,1335.7	13.25 ± 0.08	7.2 ± 0.3
Si II	1808	15.18 ± 0.02	7.2 ± 0.3
S II	1250,1259	14.73 ± 0.02	7.2 ± 0.3
Fe II	2249,2260,2374[a]	14.75 ± 0.04	7.2 ± 0.3
Zn II	2026	12.17 ± 0.03	7.2 ± 0.3

[a] Also 1608, 1611.

[b] This component is likely associated with the H_2 absorption lines observed at $z_{abs} = 2.594\,71$, 2.5 km s^{-1} blueward of $z_{abs} = 2.594\,74$.

[c] 5σ upper limit.

[d] Blend.

metal components and therefore the values for individual components may be scattered around the quoted mean. For each of the systems, we also give the Fe abundance, [Fe/H], and the metallicity, [X/H], relative to solar abundances. The metallicity was measured from the abundance of Zn when Zn II is detected, and we used either S or Si otherwise. As Zn is known to be little or undepleted on to dust grains, the [Zn/Fe] ratio should be a good indicator of dust depletion. S itself is undepleted on to dust grains. However, a possible overabundance of α-elements relative to Fe at low metallicity may lead to an overestimate of the dust-depletion factor when using [S/Fe]. However, the mean overabundance of α-elements should in general be less than approximately 0.25 dex (see Prochaska & Wolfe 2002). Si can be depleted on to dust grains and, hence, the ratio [Si/Fe] may lead to an underestimate of the dust-depletion factor, but probably by less than 0.3 dex (see Petitjean et al. 2002). In the following, however, we do not attempt to derive exact values of the dust-depletion factor but only trends in the global behaviour of the characteristics of the whole population. It will be shown that these considerations have little impact on the global results.

In Figs 11 and 12, we compare the characteristics of our sample of 33 systems (called in the following sample S1) with those of
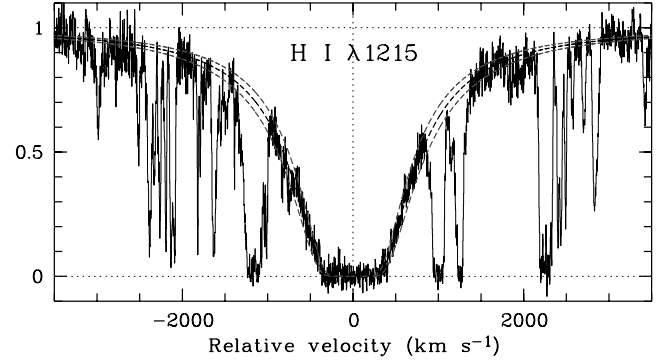
Figure 7. Portion of the normalized UVES spectrum showing the damped Lyα line of the sub-DLA system at $z_{abs} = 2.087$ toward Q 1444+014. The best-fitted Voigt profile superimposed on the data corresponds to $N(H\,I) = (1.2 \pm 0.2) \times 10^{20}$ cm^{-2}.

the global population of DLA systems. For the latter, we use the result of merging our sample with the sample of Prochaska et al. (2001). The corresponding sample will be called sample Spop and comprises 60 systems. In Fig. 11, different distributions for the global population of DLA/sub-DLA systems (sample Spop), sample S1 and the subsample of systems where H_2 is detected (sample SH$_2$) are shown.

The neutral hydrogen column density distributions are shown in the upper panel of Fig. 11. There are 28 (respectively, 32) systems with $\log N(H\,I)$ smaller (respectively, larger) than 20.6 in sample Spop, out of which 50 (respectively, 59) per cent belongs to sample S1. The two samples are statistically indistinguishable, although the mean H I column density is slightly smaller in our sample. The Kolmogorov–Smirnov test probability that the two distributions are drawn from the same parent population is $P_{KS} = 0.91$ (two-sided case). It is also apparent, although the statistics are based on a smaller data set, that there is no systematic correlation between the detection of H_2 lines and the H I column density. The $\log N(H\,I)$ distributions are similar in subsample SH$_2$ and in sample S1 ($P_{KS} > 0.9999$).

It can be seen in the middle panel of Fig. 11 that the metallicity distributions are similar in sample S1 and in the global population Spop ($P_{KS} > 0.9999$). There are 31 (respectively, 29) systems with [X/H] smaller (respectively, larger) than -1.3 in sample Spop, out of which 55 (respectively, 55) per cent are part of sample S1. However, the mean metallicity is slightly smaller in our sample. This could be a consequence of our sample including a large number of lines of sight with several DLA systems. Indeed, if these systems had a high metallicity and therefore a large dust content, they would have obscured the background quasars. However, this does not mean that these lines of sight are biased against the presence of H_2. We indeed detect H_2 at $z_{abs} = 2.595$ toward Q 0405−443, which is a line of sight containing no less than three DLA systems. The important result is that the [X/H] distributions are different in subsample SH$_2$ and in sample S1 ($P_{KS} = 0.03$): systems where H_2 is detected are definitively amongst the most metal-rich. Interestingly, none of the 17 systems with [X/H] < -1.3 in sample S1 show a detectable amount of H_2. However, H_2 is detected down to [X/H] ≈ -1.2.

The distributions of depletion factors (Fig. 11, lower panel) are also not significantly different in sample S1 compared with sample Spop ($P_{KS} = 0.98$). There are 35 (respectively, 25) systems with [X/Fe] smaller (respectively, larger) than 0.4 in sample Spop, out of which 60 (respectively, 48) per cent belongs to sample S1. Although H_2 is detected in a DLA system with [Zn/Fe] as low as 0.3 (at
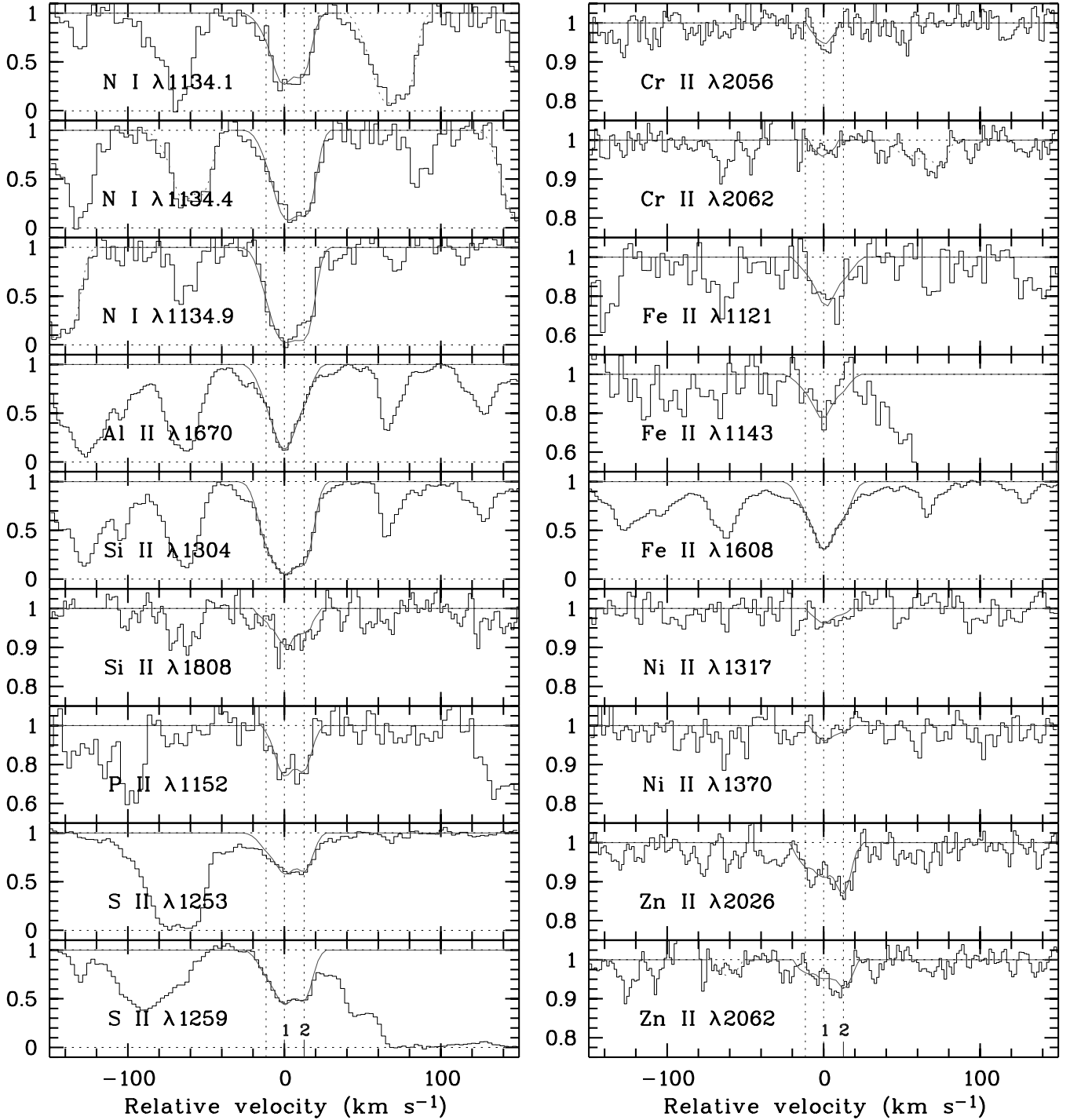
Figure 8. Velocity profiles of lines from low ions and neutral species in the sub-DLA system at $z_{abs} = 2.087$ toward Q 1444+014. Our best-fitting model of the central part of the profiles is superimposed on the spectra with vertical lines marking the location of individual components. The dotted parts in some of the synthetic profiles correspond to other transitions than those indicated. The two components where H₂ is detected are labelled with numbers 1 and 2, respectively.

$z_{abs} = 2.595$ toward Q 0405−443), there is a clear tendency for depletion factors to be larger in systems where H₂ is detected. The [X/Fe] distributions are different in subsample SH₂ and in sample S1 ($P_{KS} = 0.02$). In particular, H₂ is detected in the five systems with the largest depletion factors ([X/Fe] $\geqslant$ 0.7).

In Fig. 12, the H I column density (upper panel) and the depletion factor (lower panel) are both plotted versus metallicity. Measure-

ments from sample S1 are shown by squares, with dark squares for systems where H₂ is detected. It is apparent that, in the overall population of DLA systems, there is a lack of systems with both a high metallicity and a large H I column density. This was first noted by Boissé et al. (1998), who suggested that this might be due to the fact that, if these systems exist, they may avoid detection because the background quasars are attenuated by dust extinction (Fall &
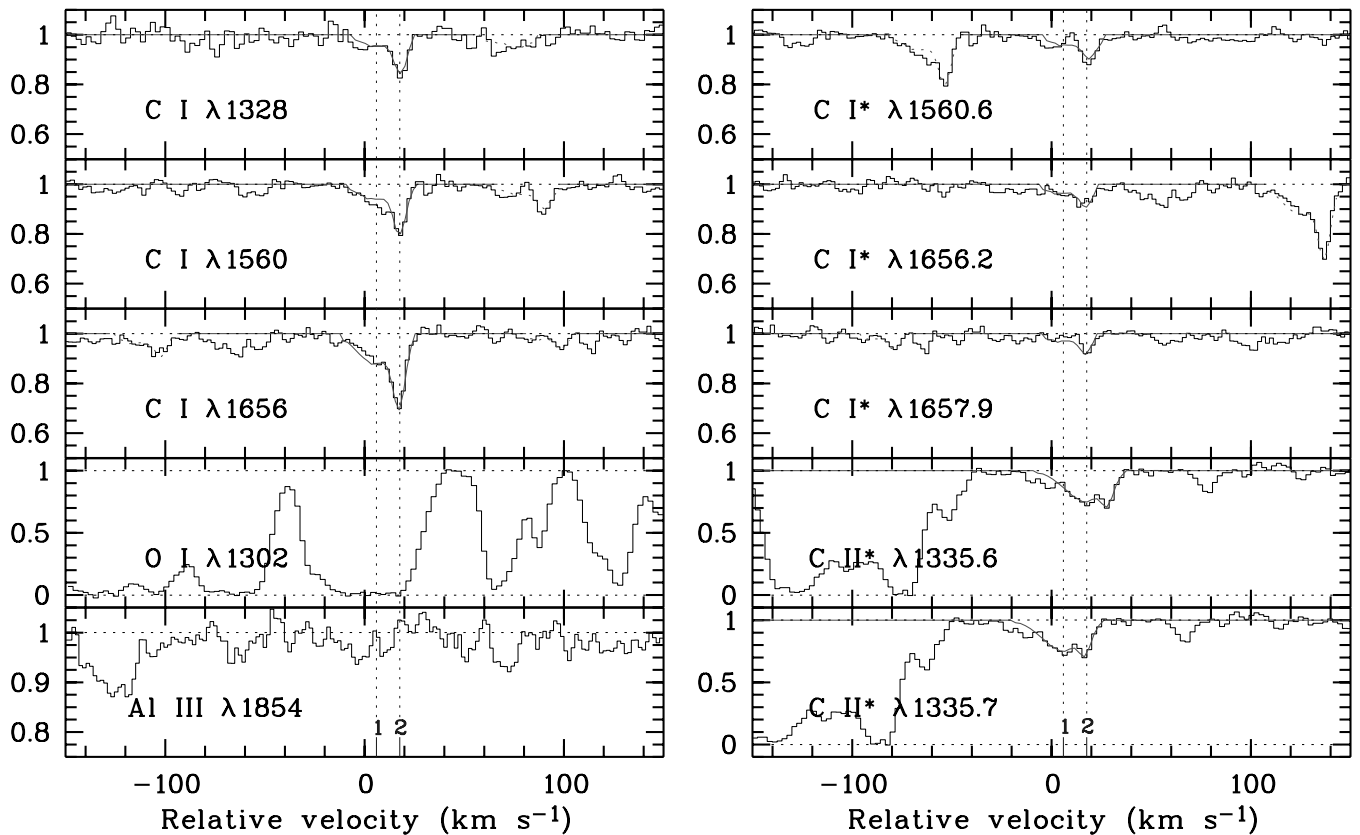
Figure 9. Absorption lines from the ground state of C I (upper part of the left-hand panel) and fine-structure levels of C I and C II (right-hand panels) at $z_{abs} = 2.087$ toward Q 1444+014. The two fitted components, where H_2 is detected, are indicated as in Fig. 8 by numbers in addition to vertical lines. The dotted parts in some of the synthetic profiles correspond to other transitions than those indicated. The origin of the velocity scale is the redshift of the main component as measured from the other metal lines ($z_{abs} = 2.08679$). The redward shift of the C I components is apparent. The velocity profile of O I $\lambda 1302$ is shown for comparison. Note that Al III $\lambda 1854$ is barely detected (bottom part of the left-hand panel) in this sub-DLA system.

Pei 1993). This assumes at least some correlation between metallicity and the amount of dust. It can be seen in the lower panel of Fig. 12 that indeed there is a trend for the most metal-rich systems to have larger depletion factors. This is detected at the 4σ significance level using a Kendall rank correlation test on censored data and taking into account the measurement uncertainties. This trend was already noted before by Ledoux et al. (2002a), at a lower significance level, probably due to a less homogenous sample, larger measurement uncertainties and the observation of a narrower metallicity range. However, from this alone, it was unclear whether this trend is a consequence of dust depletion effects or the peculiar nucleosynthesis history of zinc (Prochaska & Wolfe 2002). However, a correlation is observed in both our sample and also the global population of DLA systems. Moreover, it is clear from Fig. 12 that H_2 is detected at both the highest metallicities and the largest depletion factors. This strongly favours the fact that the correlation between metallicity and depletion factor is a consequence of dust depletion effects.

5 DISCUSSION

5.1 Molecular hydrogen in DLA systems

If we consider only DLA systems, with $\log N(\text{H I}) \geqslant 20.3$, firm detection of H_2 is achieved in six out of 24 systems. If we also include sub-DLA systems, this amounts to eight detections out of

33 systems. Therefore, H_2 is detected in more than 20 per cent of the DLA systems. However, three of the systems where H_2 is seen were already known. If we exclude these systems, we actually detect H_2 in 13–20 per cent of the newly surveyed systems. Note that we do not include in these calculations the tentative detections toward Q 0000−263 (Levshakov et al. 2000) and Q 0841+129 (Petitjean et al. 2000).

The detection probability of H_2 with column densities greater than 10^{14} cm^{-2} is more than 90 per cent along lines of sight through the interstellar medium (ISM) of our Galaxy and in the Small Magellanic Cloud (SMC) (Savage et al. 1977; Richter et al. 2001; Tumlinson et al. 2002). However, only 52 per cent of the lines of sight through the Large Magellanic Cloud (LMC) have detectable H_2 lines (Tumlinson et al. 2002). These differences in the detection probability cannot be ascribed solely to different chemical enrichment histories as the ISM of the LMC has a mean metallicity only 0.3 dex lower than the Galactic local ISM and the metallicity of the SMC is 0.6 dex lower than that (Russell & Dopita 1992). Therefore, the small detection probability in DLA systems is probably not only related to their low metallicities. The level of star formation activity in or nearby the systems might well be the primary reason for the low detection rate of H_2 as has been advocated in the case of the LMC (Kim et al. 1999).

As noted above, in our sample the detection of H_2 is not correlated with the H I column density. The H I column density distribution is similar in sample S1 and in the subsample of systems where H_2 is

Table 6. Ionic column densities in individual components of the sub-DLA system at $z_{abs} = 2.087$ toward Q 1444+014.

Ion	Transition lines used	$\log N \pm \sigma_{\log N}$	$b \pm \sigma_b$ (km s^{-1})
$z_{abs} = 2.086\,67$			
N I	1134.1,1134.4,1134.9	13.70 ± 0.10	06.1 ± 0.9
Al II	1670	11.77 ± 0.07	06.1 ± 0.9
Si II	1304,1526,1808	13.55 ± 0.08	06.1 ± 0.9
S II	1253,1259	13.79 ± 0.11	06.1 ± 0.9
Fe II	1121,1143,1608	13.18 ± 0.09	06.1 ± 0.9
Zn II	2026,2062	11.43 ± 0.18	06.1 ± 0.9
$z_{abs} = 2.086\,79$			
C I	1328,1560,1656	12.67 ± 0.09	11.6 ± 2.8
C I *	1656,1657.3,1657.9[a]	12.52 ± 0.14	11.6 ± 2.8
C II *	1335.6,1335.7	13.12 ± 0.08	11.6 ± 2.8
N I	1134.1,1134.4,1134.9	14.67 ± 0.04	06.9 ± 0.6
Mg II	1239,1240	<14.61[b]	06.9 ± 0.6
Al II	1670	12.56 ± 0.03	06.9 ± 0.6
Si II	1304,1526,1808	14.15 ± 0.06	06.9 ± 0.6
P II	1152	12.76 ± 0.06	06.9 ± 0.6
S II	1253,1259	14.32 ± 0.05	06.9 ± 0.6
Ti II	1910.6,1910.9	<12.10[b]	06.9 ± 0.6
Cr II	2056,2062,2066	12.14 ± 0.12	06.9 ± 0.6
Fe II	1121,1143,1608	13.83 ± 0.04	06.9 ± 0.6
Ni II	1317,1370	12.31 ± 0.21	06.9 ± 0.6
Zn II	2026,2062	11.66 ± 0.12	06.9 ± 0.6
$z_{abs} = 2.086\,92$			
C I	1328,1560,1656	12.82 ± 0.11	01.1 ± 0.3
C I *	1656,1657.3,1657.9[a]	12.42 ± 0.12	01.1 ± 0.3
C II *	1335.6,1335.7	12.78 ± 0.20	01.1 ± 0.3
N I	1134.1,1134.4,1134.9	14.46 ± 0.05	05.1 ± 0.5
Al II	1670	11.74 ± 0.10	05.1 ± 0.5
Si II	1304,1526,1808	13.82 ± 0.06	05.1 ± 0.5
P II	1152	12.60 ± 0.08	05.1 ± 0.5
S II	1253,1259	14.17 ± 0.06	05.1 ± 0.5
Fe II	1121,1143,1608	13.23 ± 0.09	05.1 ± 0.5
Zn II	2026,2062	11.77 ± 0.07	05.1 ± 0.5

Note: the two components of the C I, C I * and C II * profiles are redshifted by ~ 5 km s^{-1} compared with what is observed for the other metal lines (the redshifts of which are indicated).

[a] Also 1329.08, 1329.10, 1329.12, 1560.6, 1560.7.

[b] 5σ upper limit.

detected (see Fig. 11). In particular, H$_2$ is detected in two sub-DLA systems, with $\log N(\text{H\,I}) < 20.3$. In addition, among the systems where H$_2$ is detected there is no correlation between the logarithm of the molecular fraction, $\log f$, and $\log N(\text{H\,I})$ (see Fig. 13).

In Fig. 13, confirmed detections and upper limits on the molecular fraction in sample S1 are represented by, respectively, dark and shaded squares. Observations along lines of sight in the LMC and SMC from Tumlinson et al. (2002) and in the Galaxy from Savage et al. (1977) are also shown. It is apparent that most DLA systems are similar to the LMC and/or SMC lines of sight. In particular, and contrary to what happens in our Galaxy, a significant number of lines of sight through the LMC have $\log f < -6$ for $20.5 \leqslant \log N(\text{H\,I}) \leqslant 21.5$. This is also the case for 58 per cent of the DLA systems [$20.3 \leqslant \log N(\text{H\,I}) \leqslant 21.7$] in which we could achieve such a limit, which means that this number is a lower limit on the fraction of systems having such a small molecular fraction. Indeed, if all detection limits are considered to be that constraining then the fraction of systems with $\log f < -6$ is 75 per cent. Note that several systems have a very small molecular fraction, $\log f \lesssim -7$. Interestingly, this is an order

of magnitude smaller than the primordial freeze-out fraction of H$_2$ molecules (Lepp & Shull 1984). It is very difficult to reproduce such small values in models of cool clouds (see Petitjean et al. 2000; Liszt 2002). When H$_2$ is detected, the molecular fraction is in the range $-3 < \log f < -1$ with some scatter, with the exception of the DLA system toward Q 0347$-$383 for which $\log f = -5.71$. The former values are similar to what is seen along the LMC and SMC lines of sight.

The sharp transition from $\log f < -4$ to $\log f > -2$ at a column density $\log N(\text{H\,I}) \approx 20.7$ observed for the Galactic lines of sight (Savage et al. 1977) is not clearly present in the SMC, in the LMC nor in sample SH$_2$. This transition is believed to occur at the point at which the clouds achieve self-shielding. However, a characteristic H I column density can possibly correspond to some self-shielding scale only if the parameters controlling the formation equilibrium of H$_2$ are similar along different lines of sight, with very little scatter, which may be the case in our Galaxy. Therefore, our results suggest that DLA systems span a wide range of physical conditions. This is also suggested by the large scatter seen in the metallicity measured in DLA systems at a given redshift (see, e.g., Prochaska & Wolfe 2002). This conclusion is strengthened by the fact that there is a clear dichotomy in $\log f$ values whatever the H I column density, with very few measurements in the range $-5 < \log f < -3$. This bi-modal distribution could be a consequence of self-shielding, which would mean that, in DLA systems, self-shielding can be achieved at any H I column density probably because the UV radiation field varies strongly from one system to the other. Alternatively, as shown by Tumlinson et al. (2002) in the case of the Magellanic Clouds, most of the observations can be explained by models where the formation rate of H$_2$ on to dust grains is reduced and the ionizing flux is enhanced relative to what is observed in our Galaxy (see also the models by Schaye 2001). Basically, the above characteristic H I column density, $\log N(\text{H\,I}) = 20.7$, observed for Galactic clouds, would be located beyond the observed range in the case of DLA systems [i.e. $\log N(\text{H\,I}) \gtrsim 21.8$].

Note that there are two sub-DLA systems, with $\log N(\text{H\,I}) < 20.3$, having detected H$_2$ molecules. These systems, at $z_{abs} = 1.968$ toward Q 0013$-$004 and $z_{abs} = 2.087$ toward Q 1444+014, are amongst the most metal (and dust) -rich absorbers of sample S1. They, together with the DLA system at $z_{abs} = 2.338$ toward Q 1232+082, have the highest molecular fractions, and could be part of the population arising in Galactic disc-like gas.

5.2 The role of dust

It can be seen in Fig. 11 that the probability of detecting H$_2$ is unity for systems with large depletion factors, [X/Fe] $\geqslant 0.7$. This is a crude indication that the presence of dust is an important factor for the formation of H$_2$ in DLA systems. It is known that H$_2$ formation is mediated by either dust grains if the gas is cool and dense or H$^-$ if it is warm and dust-free. If the former process is dominant in DLA systems then some correlation between the H$_2$ molecular fraction and the amount of dust is expected. However, in the case of DLA systems it is difficult to quantify the amount of dust that is present. We first plot in Fig. 14 molecular fractions versus depletions (probably on to dust grains) as estimated from the abundances of Zn relative to Fe, or S when Zn is not detected, or Si when Zn is not detected and sulphur lines are blended. A trend between both quantities is present at the 3.6σ significance level using a Kendall rank correlation test, taking into account upper and lower limits on $\log f$. Note, however, that there is a two orders of magnitude scatter in $\log f$ for a given depletion factor so that there is basically no
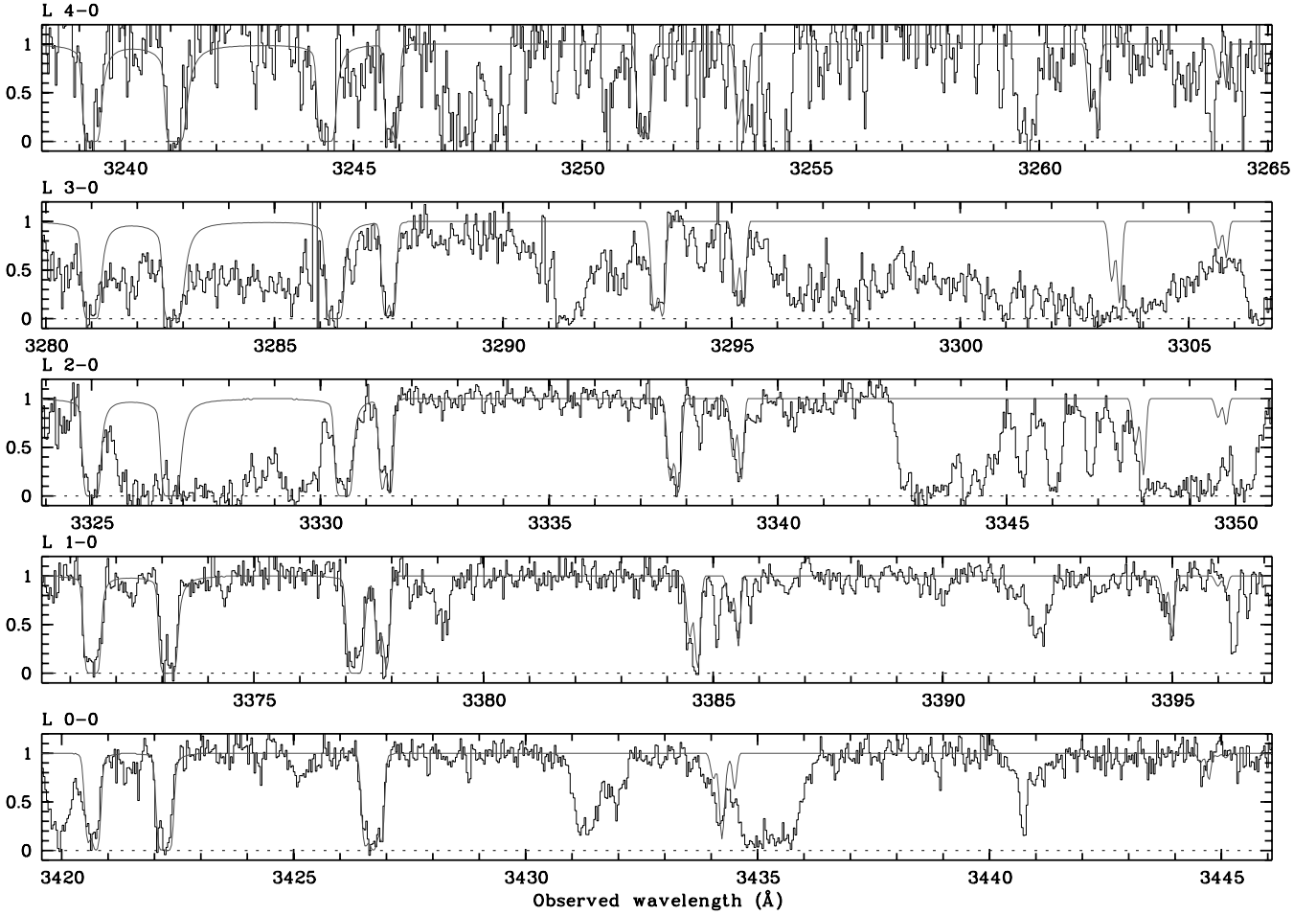
Figure 10. Voigt-profile fitting to the transition lines from the $J = 0, 1, 2, 3$ and 4 rotational levels of the vibrational ground-state Lyman band of H_2 at $z_{abs} \approx 2.087$ toward Q 1444+014. H_2 is detected on this line of sight in two gas clouds spanning 12 km s^{-1} in velocity space.

Table 7. Voigt-profile fitting results for different rotational levels of the vibrational ground-state Lyman band of H_2 toward Q 1444+014.

z_{abs}	Level	$\log N \pm \sigma_{\log N}$ (H$_2$)	$b \pm \sigma_b$ (km s^{-1})
2.086 80	$J = 0$	$15.68^{+0.22}_{-0.08}$	5.5 ± 0.5
	$J = 1$	$16.37^{+0.27}_{-0.11}$	5.5 ± 0.5
	$J = 2$	$15.31^{+0.06}_{-0.03}$	5.5 ± 0.5
	$J = 3$	$14.80^{+0.06}_{-0.04}$	5.5 ± 0.5
	$J = 4$	$\leqslant 14.15^a$	5.5 ± 0.5
	$J = 5$	$< 13.75^b$	5.5 ± 0.5
2.086 96	$J = 0$	$17.46^{+0.10}_{-0.11}$	2.6 ± 0.6
	$J = 1$	$18.03^{+0.12}_{-0.12}$	2.6 ± 0.6
	$J = 2$	$16.63^{+0.57}_{-0.46}$	2.6 ± 0.6
	$J = 3$	$15.26^{+0.07}_{-0.08}$	2.6 ± 0.6
	$J = 4$	$\leqslant 14.20^a$	2.6 ± 0.6
	$J = 5$	$< 13.75^b$	2.6 ± 0.6

Note: errors in the column densities correspond to a range of column densities; they are not the rms errors from fitting the Voigt profiles (see the text).
^{a}Possible blends.
$^b5\sigma$ upper limit.

correlation between $\log f$ and [X/Fe] if only detections are considered (correlation significant at the $\lesssim 1\sigma$ level only). The above trend is therefore a consequence of H_2 being detected in none of the systems with [X/Fe] < 0.4 except one (at $z_{abs} = 2.595$ toward Q 0405−443). The corresponding systems have a very low dust content. A depletion factor [Zn/Fe] ~ 0.4 corresponds to a very small $E(B - V)$ (~ 0.01) for physical conditions similar to those prevailing in our Galaxy. We have seen that the depletion factor is correlated with the metallicity in DLA systems. There is therefore some correlation between the depletion factor and the amount of dust. However, the scatter is large. This is why it can be, in general, misleading to use only the depletion factor as an indicator of the dust content of the absorbing gas.

A better indicator of the dust content is the dust-to-gas ratio: $\kappa_X = 10^{[X/H]}(1 - 10^{[Fe/X]})$, where X stands for a reference element that is little or unaffected by dust depletion effects. In Fig. 15, we plot the molecular fraction versus the amount of dust as measured by the dust-to-gas ratio. It can be seen that, as expected, low dust content, $\log \kappa_X < -1.5$ (e.g. [X/H] < -1.3 and [X/Fe] < 0.5), implies a low molecular fraction, $\log f < -5$, while a larger molecular fraction, $\log f \gtrsim -4$, is only found for higher dust content, $\log \kappa_X > -1.5$. However, large amounts of dust do not always imply large molecular fractions. There are a few non-detections with $\log \kappa_X > -1.5$ and $\log f < -5$. In particular, the two systems with $\log \kappa_X \simeq -0.5$ and $\log f < -5$ are sub-DLA systems (see also Fig. 12, upper plot, at

Table 8. Summary of molecular and metal contents in the H$_2$-survey sample of DLA/sub-DLA systems.

QSO	z_{em}	z_{abs}	log N(H I)	log N(H$_2$)[1]		log f[2]	[Fe/H][3]	[X/H][3]	X
				$J = 0$	$J = 1$				
0000−263	4.10	3.390	21.41 ± 0.08[a]	<13.9	13.74::[b]	<−6.98	-2.05 ± 0.09[c]	-2.05 ± 0.09[c]	Zn
0010−002	2.14	2.025	20.80 ± 0.10	<14.0	<14.2	<−6.09	-1.25 ± 0.11	-1.20 ± 0.12	Zn
0013−004	2.09	1.968	$\leqslant 19.43$[d]	$16.77^{+0.05}_{-0.07}$[d]		$\geqslant -2.36$[d]	$\geqslant -2.33$[d,4]	$\geqslant -0.73$[d,4]	Zn
0013−004	2.09	1.973	20.83 ± 0.05[d]	17.72 / 20.00[d]		−2.81 / −0.64[d]	-1.75 ± 0.05[d]	-0.93 ± 0.06[d]	Zn
0058−292	3.09	2.671	21.00 ± 0.10	<13.8	<13.6	<−6.69	-1.76 ± 0.10	-1.42 ± 0.11	Zn
0102−190	3.04	2.370	20.85 ± 0.08	<14.7	<14.6	<−5.60	-1.89 ± 0.13	-1.73 ± 0.14	Zn
0112−306	2.98	2.418	20.37 ± 0.08	<13.8	<14.2	<−5.72	-2.50 ± 0.09	-2.31 ± 0.08	Si
0112−306	2.98	2.702	20.15 ± 0.07	<14.1	<14.0	<−5.50	-0.89 ± 0.10	-0.33 ± 0.11	Si
0112+029	2.81	2.423	20.70 ± 0.10	<13.6	<13.9	<−6.32	-1.35 ± 0.11	-1.14 ± 0.13	S
0135−273	3.21	2.800	20.80 ± 0.10	<13.8	<13.8	<−6.40	-1.54 ± 0.15	-1.29 ± 0.17	S
0347−383	3.22	3.025	20.56 ± 0.05	14.55 ± 0.09		-5.71 ± 0.10	-1.72 ± 0.06	-0.98 ± 0.09	Zn
0405−443	3.02	2.550	21.00 ± 0.15	<13.9	<13.7	<−6.59	-1.52 ± 0.15	-1.17 ± 0.16	Zn
0405−443	3.02	2.595	20.90 ± 0.10	$18.16^{+0.21}_{-0.06}$		$-2.44^{+0.23}_{-0.12}$	-1.33 ± 0.11	-1.02 ± 0.12	Zn
0405−443	3.02	2.621	20.25 ± 0.10	<13.5	<13.5	<−6.15	-2.15 ± 0.10	-1.83 ± 0.10	Si
0528−250	2.78	2.811	21.10 ± 0.10	$18.22^{+0.23}_{-0.16}$[5]		$-2.58^{+0.25}_{-0.19}$[5]	-1.26 ± 0.10	-0.75 ± 0.10	Zn
0551−366	2.32	1.962	20.50 ± 0.08[e]	$17.42^{+0.63}_{-0.90}$[e]		$-2.78^{+0.64}_{-0.90}$[e]	-0.96 ± 0.09[e]	-0.13 ± 0.09[e]	Zn
0841+129	2.50	2.374	20.90 ± 0.10	14.56::	<14.0	<−5.93	-1.71 ± 0.11	-1.52 ± 0.14	Zn
0841+129	2.50	2.476	20.65 ± 0.10	<14.0	<14.0	<−6.05	-1.51 ± 0.11	-1.52 ± 0.11	S
1037−270	2.23	2.139	19.70 ± 0.10[f]	<13.7[f]	<13.7[f]	<−5.40[f]	-0.65 ± 0.10[f]	-0.26 ± 0.11[f]	Zn
1101−264	2.14	1.839	19.35 ± 0.04	<14.0	<14.0	<−4.75	-1.36 ± 0.05	-0.82 ± 0.14	S
1117−133	3.96	3.351	20.85 ± 0.10[g]	<13.7	<14.0	<−6.37	-1.55 ± 0.13[g]	-1.28 ± 0.13[g]	Zn
1157+014	1.99	1.944	21.70 ± 0.10	<14.3	<14.5	<−6.69	-1.73 ± 0.10	-1.32 ± 0.10	Zn
1223+178	2.94	2.466	21.40 ± 0.10	<14.0	<14.0	<−6.80	-1.70 ± 0.10	-1.63 ± 0.11	Zn
1232+082	2.58	2.338	20.90 ± 0.10[h]	$\geqslant 17.19$[h,6]		$\geqslant -3.41$[h,6]	-1.73 ± 0.13[h]	-1.21 ± 0.15[h]	Si
1337+113	2.92	2.508	19.95 ± 0.05	<13.8	<14.1	<−5.37	-2.05 ± 0.07	-1.59 ± 0.09	Si
1337+113	2.92	2.796	20.85 ± 0.08	<13.6	<13.8	<−6.54	-2.02 ± 0.09	-1.69 ± 0.11	Si
1444+014	2.21	2.087	20.07 ± 0.07	$18.30^{+0.37}_{-0.37}$		$-1.48^{+0.38}_{-0.38}$	-1.58 ± 0.09	-0.60 ± 0.15	Zn
1451+123	3.25	2.469	20.30 ± 0.10	<15.0:	<15.0:	<−4.70	-2.41 ± 0.10	-1.98 ± 0.14	Si
1451+123	3.25	3.171	19.90 ± 0.20	<13.5	<13.5	<−5.80	-2.09 ± 0.24	-1.83 ± 0.21	Si
2059−360	3.09	2.508	20.14 ± 0.07	<14.7	<14.5	<−4.93	-2.12 ± 0.08	-1.76 ± 0.09	S
2059−360	3.09	3.083	20.85 ± 0.08	<13.5	<13.7	<−6.64	-1.83 ± 0.09	-1.65 ± 0.12	S
2138−444	3.17	2.852	20.82 ± 0.05	<13.5	<13.1	<−6.87	-1.68 ± 0.05	-1.48 ± 0.05	Zn
2332−094	3.30	3.057	20.30 ± 0.08	<12.8	<13.1	<−6.72	-1.47 ± 0.08	-1.49 ± 0.20	S

[1] We give total molecular hydrogen column densities summed up over all J levels in case of detection and upper limits for $J = 0$ and 1 in the case of non-detection.

[2] Molecular fraction $f = 2N(H_2)/[2N(H_2) + N(H I)]$.

[3] Fe abundances, [Fe/H], and metallicities, [X/H] with either X = Zn, S or Si. In order to derive meaningful abundance ratios, the components taken into account in the profiles are those simultaneously detected in the weak lines of Zn II, S II and Si II (see Ledoux et al. 2002a).

[4] [Zn/Fe] $= 1.60 \pm 0.04$.

[5] The fitting was performed on the new UVES data taking into account the two-component structure of the cloud.

[6] The total H$_2$ column density of this system will be derived from higher quality data. The value derived by Srianand et al. (2000) should be considered as a lower limit.

References: hydrogen column density and metal abundance measurements are from this work, unless otherwise indicated: (a) Lu et al. (1996); (b) Levshakov et al. (2001); (c) Molaro et al. (2001); (d) Petitjean et al. (2002); (e) Ledoux et al. (2002b); (f) Srianand & Petitjean (2001); (g) Péroux et al. (2002); (h) Srianand et al. (2000).

[X/H] $\simeq -0.3$). Therefore, in these systems the lack of molecules could be a consequence of an enhanced radiation field below the Lyman limit.

Another important factor governing the presence of H$_2$ molecules appears to be the local physical conditions of the absorbing gas. Relatively large molecular fractions, log $f > -4$, are found in gas having large particle densities, $n_H > 20$ cm^{-3}, and low temperatures, $T < 300$ K (see Ledoux et al. 2002b; Petitjean et al. 2002). One should bear in mind that the formation rate of H$_2$ goes linearly with the density of dust grains, while it goes as the second power of the H I density. Therefore, it is natural that, even though the presence of dust is an important factor for the formation of molecules, local physical conditions such as gas density, temperature and local UV field play a major role in governing the molecular fraction of a given cloud in DLA systems.

Note that the above discussion is based on the determination of mean metallicities in DLA systems. In most cases, this means that the metallicity is calculated over some velocity range and, therefore, over several components. However, we have shown that the depletion in the components where H$_2$ is detected can be much larger than the mean depletion. As an example, a large depletion factor has been observed in a well-defined, weak H$_2$ component in the DLA system at $z_{abs} = 1.97$ toward Q 0013−004 (Petitjean et al. 2002). This kind of component can usually be revealed by the
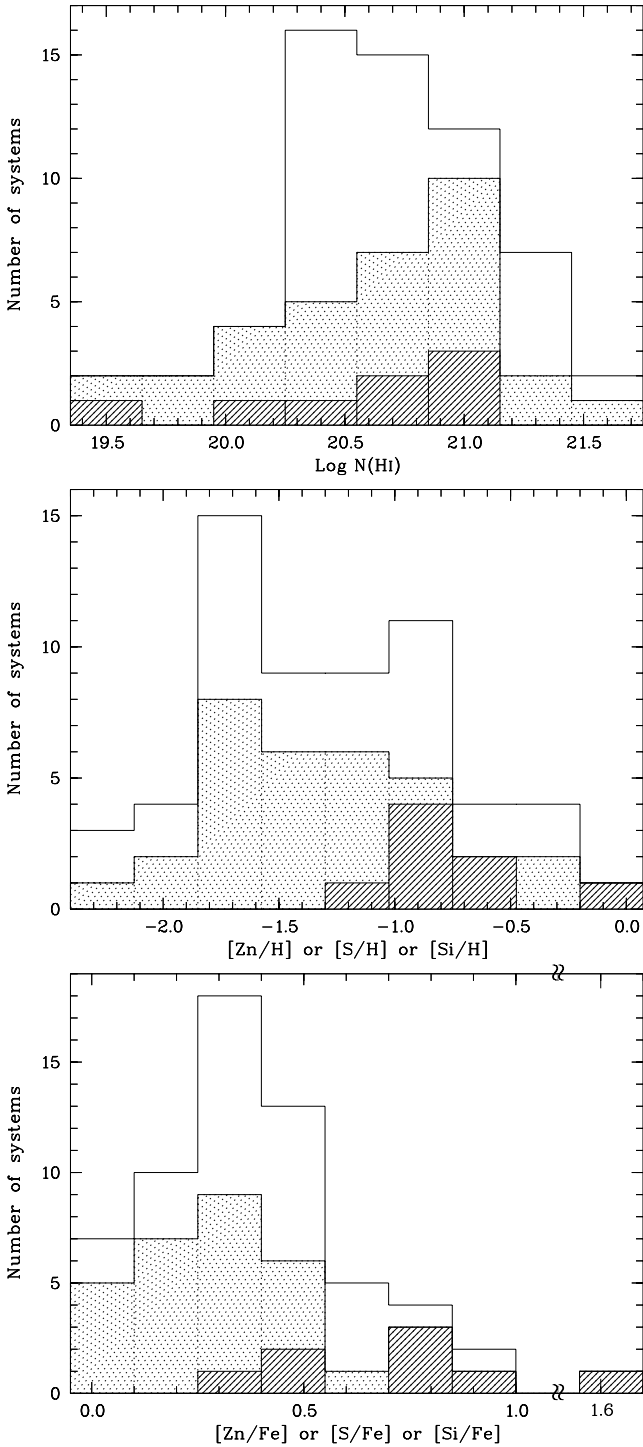
Figure 11. Distributions of neutral hydrogen column densities (upper panel), metallicities (middle panel; measured from either [Zn/H], [S/H] or [Si/H]) and depletion factors (lower panel; measured from either [Zn/Fe], [S/Fe] or [Si/Fe]) in, respectively, the global population of DLA/sub-DLA systems (overall distribution), our H_2-survey sample (dotted histogram) and the subsample of H_2-detected systems (hashed histogram).

Figure 12. Neutral hydrogen column density (upper plot) and depletion factor (lower plot) versus metallicity in, respectively, the global population of DLA/sub-DLA systems (all symbols), our H_2-survey sample (all squares) and the subsample of H_2-detected systems (dark squares). The typical error bars are shown in the upper-left part of each plot. A correlation between metallicity and depletion factor is present at the 4σ significance level, confirming the trend previously detected by Ledoux et al. (2002a).

corresponding, narrow C I absorption line. However, for other species the component is most often blended with other components in the rest of the profile. This means that absorption lines due to cold gas, i.e. related to C I components, can be hidden in the absorption-line profile produced by a more pervasive

medium. This implies that absolute metallicities are not accurately determined in the cold gas. This fact is probably not important for volatile elements as for them the dominant components actually produce the strongest absorption lines, but could be of importance for Fe co-production elements, which can be depleted on to dust grains. Consequently, absorption lines from the latter elements can be weak and lost in the profiles. Therefore, we could underestimate the depletion factors in these components.

5.3 Evolution with redshift

In the previous section, we have given two new arguments in favour of the presence of dust in DLA systems. First, there is a correlation between metallicity and depletion factor and, secondly, molecular
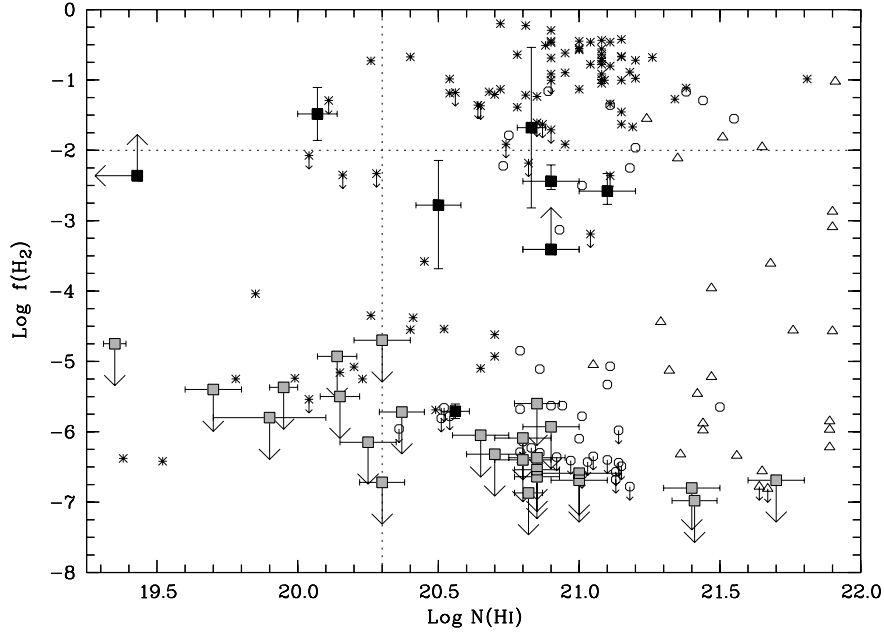
Figure 13. Mean H_2 molecular fraction $f = 2N(H_2)/[2N(H_2) + N(H\,\textsc{i})]$ versus neutral hydrogen column density. Measurements in DLA/sub-DLA systems are indicated by dark squares for H_2 detections and shaded ones for upper limits. Observations along lines of sight in the Galaxy (Savage et al. 1977) and the LMC and SMC (Tumlinson et al. 2002) are indicated by, respectively, asterisks, circles and triangles.
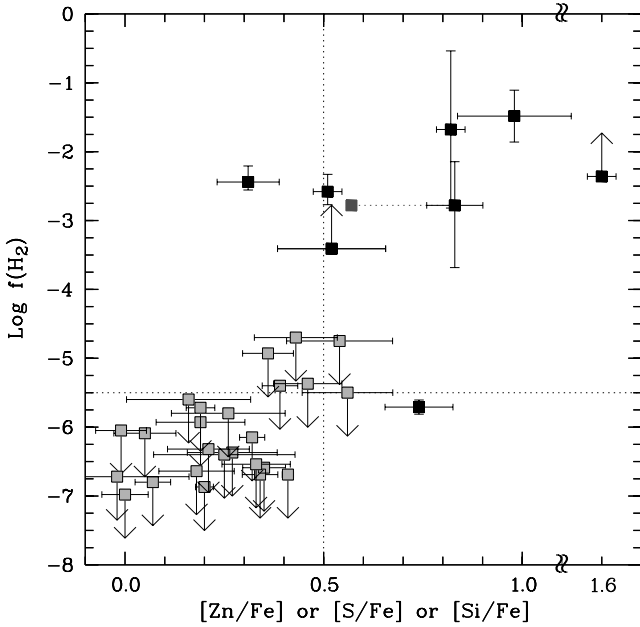

Figure 14. Mean H_2 molecular fraction versus depletion on to dust grains as estimated from the abundance of either $X = $ Zn, S or Si relative to Fe, in the H_2-survey sample (see Table 8). H_2 detections, measured by our group, are indicated by dark squares. The dotted line segment links data points for the DLA system toward Q 0551−366 considering either [Fe/Zn] or [Fe/S]. This is indeed the only one case where the difference between measured [X/Fe] ratios is significantly larger than 0.1 dex (i.e. 0.24 dex). The two dotted lines are drawn for illustrative purposes (see the text).
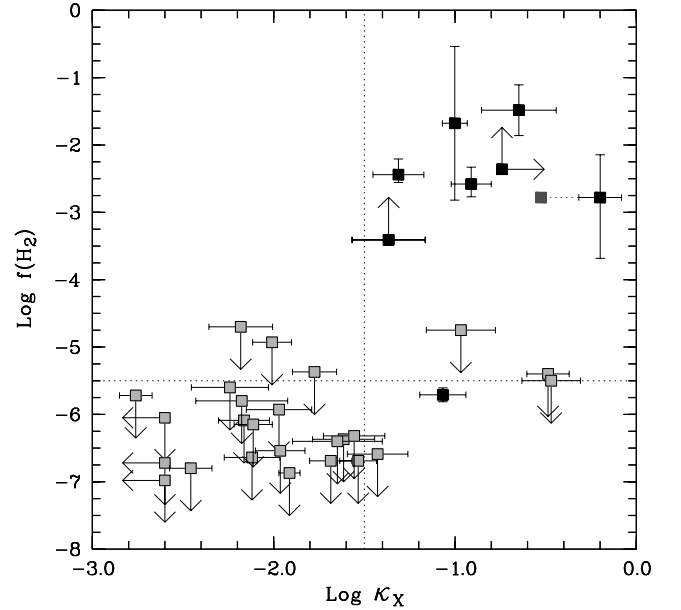
Figure 15. H_2 molecular fraction versus the amount of dust or dust-to-gas ratio $\kappa_X = 10^{[X/H]}(1 - 10^{[Fe/X]})$, with either $X = $ Zn, S or Si. Drawing conventions are the same as in Fig. 14. A weak trend between the two quantities is apparent; however, several orders of magnitude spread in $f(H_2)$ for a given dust content, among the detected cases, suggests that in addition to the amount of dust the physical conditions of the gas (density, temperature, UV flux) play an important role in governing the formation of H_2 in DLA systems.

hydrogen is observed in the systems having the highest metallicities and the largest depletion factors. In a simple picture of star formation history, one can imagine that the gas is slowly enriched by on-going star formation and, therefore, metallicity and dust content should

increase together with time. In Fig. 16, we plot the total number of DLA/sub-DLA systems in our sample versus redshift along with the number of systems where H_2 is detected. Although the statistics are based on small numbers, the probability of finding molecules in the
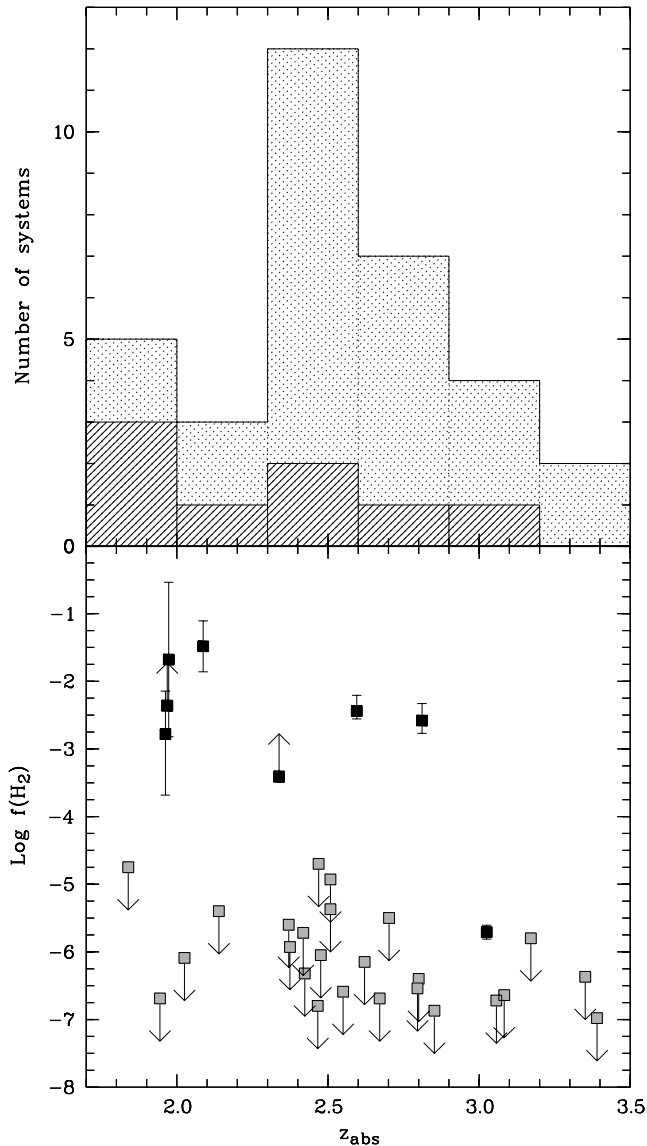
Figure 16. Upper panel, redshift distribution of the DLA/sub-DLA systems in our sample. The subsample of H_2-detected systems is indicated by the hashed histogram. Lower panel, H_2 molecular fraction versus redshift. Detections are shown by dark squares and upper limits by shaded ones. Although the statistics are based on small numbers, the probability of finding molecules at $z_{abs} \sim 2$ is highest. This probably reveals that the amount of dust in DLA systems increases with time.

$z_{abs} \sim 2$ systems is highest. This probably indicates that the amount of dust in DLA systems increases with time. Although increasing Zn metallicity with decreasing redshift is not fully established (e.g. Pettini et al. 1999), there is some evidence for such an increase at $z_{abs} < 3.5$ (Kulkarni & Fall 2002; Prochaska & Wolfe 2002). Consequently, the possible lack of increase with time of the mean Fe metallicity in DLA systems (e.g. Prochaska & Wolfe 2002) could be related to the fact that the intrinsic increase in metallicity is hidden by larger depletion on to dust grains at low and intermediate redshifts (see Ledoux et al. 2002a).

6 CONCLUSIONS

Although the presence of dust in DLA systems was claimed very early on (Pei, Fall & Bechtold 1991), the issue of whether the abun-

dance pattern observed in DLA systems reflects depletion of refractory elements on to dust grains or nucleosynthesis effects has remained controversial (see, e.g., Lu et al. 1996; Pettini et al. 1997). Recently, several studies have shown that the two effects, dust depletion and peculiar nucleosynthesis history, should be invoked altogether to explain the observations (Vladilo 1998; Ledoux et al. 2002a; Prochaska & Wolfe 2002). In any case, all of these studies conclude that the dust content of DLA systems is usually small. However, it is possible that the current sample of DLA systems is biased against high-metallicity and dusty absorbers. Indeed, Boissé et al. (1998) have noted that there is a lack of absorbers with both a large $N(\text{H\,{\sc i}})$ and a high metallicity. If this dust-induced bias exists, however, it probably cannot lead to an underestimate of the H\,{\sc i} mass in DLA systems by more than a factor of 2 (Ellison et al. 2001).

In the course of a survey of 24 DLA and nine sub-DLA systems, we have confirmed four previous detections of molecular hydrogen and made three new ones. The bulk of the DLA population is found to have low metallicities, $[X/H] < -1.0$, together with small depletion factors, $[X/Fe] < 0.5$. Although molecules can be found along lines of sight with small depletion factors ($[Zn/Fe] = 0.3$), they are generally found in the most metal-rich systems, $[X/H] > -1.0$, with large depletion factors, $[X/Fe] > 0.5$. This clearly demonstrates the existence of dust in at least 20 per cent of the DLA systems. Moreover, we have found very large depletion factors in two subsystems where H_2 is detected, at $z_{abs} = 1.96822$ toward Q 0013−004 (Petitjean et al. 2002), where $[Zn/Fe] = 1.6$, and at $z_{abs} = 2.08692$ toward Q 1444+014 (see Subsection 3.3), where $[Zn/Fe] = 1.4$. This shows that dust depletion can be quite large in some of the DLA systems. The extinction is small in these cases, however, probably because of relatively small H\,{\sc i} column densities [e.g. log $N(\text{H\,{\sc i}}) < 19.5$ in the $z_{abs} = 1.96822$ system toward Q 0013−004]. In addition, there is a correlation between the metallicity and the depletion factor in all DLA samples (large depletion factors are seen in systems with high metallicities). This trend has been noted before by Ledoux et al. (2002a). However, it was unclear whether this trend is really due to dust depletion. Prochaska & Wolfe (2002) indeed argued that such a correlation may arise from a significant dispersion in the production of zinc. However, the correlation is present in both our sample and also the global population of DLA systems. Moreover, it is clear that molecular hydrogen is mostly detected at the highest metallicities and the largest depletion factors. This strongly favours the hypothesis that the correlation between the metallicity and the depletion factor is actually a consequence of dust depletion effects. Not only could dust be present in most of the DLA systems, but also the possibility that the population of DLA systems is biased against the presence of systems having both a high metallicity and a large dust content still needs to be considered seriously.

One of the striking results of the survey is that for most of the DLA systems the molecular fraction is very small (log $f < -6$). This is much smaller than what is observed in the disc of the Galaxy at similar H\,{\sc i} column densities (see Savage et al. 1977). However, the situation is comparable to what is observed along lines of sight in the LMC and SMC (Tumlinson et al. 2002). Indeed, similar upper limits on the molecular fraction have been measured for a large number of lines of sight in the LMC. Moreover, the mean molecular fraction in DLA systems where H_2 is detected is of the order of 0.01, approximately the same as in the LMC and SMC, and approximately a factor of 10 smaller than in the disc of the Galaxy. This is probably a consequence of reduced formation rate of H_2 on to dust grains because the temperature of the gas is high (Petitjean et al. 2000).

Indeed, within the framework of models of cool clouds it is difficult to explain the very low values of the upper limits (log $f \lesssim -7$) achieved for a handful of DLA systems in our sample (see fig. 7 of Liszt 2002). This could also be due to an intense ambient UV flux (see models by Tumlinson et al. 2002), but this is unclear and should be investigated by detailed analysis of the systems where H$_2$ is detected (see Srianand & Petitjean 1998; Ledoux et al. 2002b; Petitjean et al. 2002).

Star formation activity is probably not intense in the close vicinity of most of the systems. Møller et al. (2002) found that a few DLA systems are associated with Lyman-break galaxies. However, from spectroscopy of 11 out of 22 candidates in six fields, targeting eight DLA systems, they identified only one galaxy counterpart. This means that, even if DLA systems can be associated with Lyman-break galaxies, most of the time they must have moderate star formation activity with luminosities $L < L^*$ (see, e.g., Fynbo, Møller & Thomsen 2001). In addition, within the framework of current models of structure formation, DLA systems preferentially sample the outer regions of galaxies at the faint end of the galaxy luminosity function (Haehnelt et al. 2000). One way of explaining the small molecular fractions observed in DLA systems is that the associated emitting object is faint and has moderate star formation activity, but that the gas giving rise to the DLA absorption line is located inside the regions where star formation occurs. The probably large turbulence induced by on-going star formation may then help explain the required large covering factors associated with such regions. This would imply that star formation is gentle and diffuse in the systems. The diffuse UV flux can be estimated from the excitation of molecular hydrogen. This will be performed in a forthcoming paper. Additional deep imaging in the vicinity of the QSO lines of sight is also needed to unveil the nature of star formation activity in DLA systems.

ACKNOWLEDGMENTS

REFERENCES

Ballester P., Modigliani A., Boitquin O., Cristiani S., Hanuschik R., Kaufer A., Wolf S., 2000, Messenger, 101, 31

Bergeson S.D., Lawler J.E., 1993a, ApJ, 408, 382

Bergeson S.D., Lawler J.E., 1993b, ApJ, 414, L137

Black J.H., Chaffee F.H., Jr, Foltz C.B., 1987, ApJ, 317, 442

Boissé P., Le Brun V., Bergeron J., Deharveng J.-M., 1998, A&A, 333, 841

Cazaux S., Tielens A.G.G.M., 2002, ApJ, 575, L29

Dekker H., D'Odorico S., Kaufer A., Delabre B., Kotzlowski H., 2000, in Iye M., Moorwood A.F., eds, Proc. SPIE Vol. 4008, Optical and IR Telescope Instrumentation and Detectors. Int. Soc. Opt. Eng., Bellingham, WA, p. 534

Ellison S.L., Yan L., Hook I.M., Pettini M., Wall J.V., Shaver P., 2001, A&A, 379, 393

Fall S.M., Pei Y.C., 1993, ApJ, 402, 479

Fedchak J.A., Lawler J.E., 1999, ApJ, 523, 734

Fedchak J.A., Wiese L.M., Lawler J.E., 2000, ApJ, 538, 773

Federman S.R., Beideck D.J., Schectman R.M., York D.G., 1992, ApJ, 401, 367

Foltz C.B., Chaffee F.H., Jr, Black J.H., 1988, ApJ, 324, 267

Fynbo J.U., Møller P., Thomsen B., 2001, A&A, 374, 443

Gardner J.P., Katz N., Hernquist L., Weinberg D.H., 2001, ApJ, 559, 131

Ge J., Bechtold J., 1997, ApJ, 477, L73

Ge J., Bechtold J., 1999, in Carilli C.L., Radford S.J.E., Menten K.M., Langston G.I., eds, ASP Conf. Ser. Vol. 156, Highly Redshifted Radio Lines. Astron. Soc. Pac., San Francisco, p. 121

Ge J., Bechtold J., Kulkarni V.P., 2001, ApJ, 547, L1

Haehnelt M.G., Steinmetz M., Rauch M., 2000, ApJ, 534, 594

Howk J.C., Sembach K.R., Roth K.C., Kruk J.W., 2000, ApJ, 544, 867

Jenkins E.B., Peimbert A., 1997, ApJ, 477, 265

Jenkins E.B., Shaya E.J., 1979, ApJ, 231, 55

Kim S., Dopita M.A., Staveley-Smith L., Bessell M.S., 1999, AJ, 118, 2797

Kulkarni V.P., Fall S.M., 2002, ApJ, 580, 732

Ledoux C., Bergeron J., Petitjean P., 2002a, A&A, 385, 802

Ledoux C., Srianand R., Petitjean P., 2002b, A&A, 392, 781

Lepp S., Shull J.M., 1984, ApJ, 280, 465

Levshakov S.A., Varshalovich D.A., 1985, MNRAS, 212, 517

Levshakov S.A., Chaffee F.H., Foltz C.B., Black J.H., 1992, A&A, 262, 385

Levshakov S.A., Molaro P., Centurión M., D'Odorico S., Bonifacio P., Vladilo G., 2000, A&A, 361, 803

Levshakov S.A., Molaro P., Centurión M., D'Odorico S., Bonifacio P., Vladilo G., 2001, in Cristiani S., Renzini A., Williams R.E., eds, ESO/ECF/STScI Workshop, Deep Fields. Springer-Verlag, Berlin, p. 334

Levshakov S.A., Dessauges-Zavadsky M., D'Odorico S., Molaro P., 2002, ApJ, 565, 696

Liszt H., 2002, A&A, 389, 393

Lopez S., Ellison S.L., 2003, A&A, 403, 573

Lopez S., Maza J., Masegosa J., Marquez I., 2001, A&A, 366, 387

Lu L., Sargent W.L.W., Barlow T.A., Churchill C.W., Vogt S.S., 1996, ApJS, 107, 475

Molaro P., Levshakov S.A., D'Odorico S., Bonifacio P., Centurión M., 2001, ApJ, 549, 90

Møller P., Warren S.J., Fall S.M., Fynbo J.U., Jakobsen P., 2002, ApJ, 574, 51

Morton D.C., 1991, ApJS, 77, 119

Morton D.C., Dinerstein H.L., 1976, ApJ, 204, 1

Pei Y.C., Fall S.M., Bechtold J., 1991, ApJ, 378, 6

Péroux C., Petitjean P., Aracil B., Srianand R., 2002, New Astron., 7, 577

Petitjean P., Srianand R., Ledoux C., 2000, A&A, 364, L26

Petitjean P., Srianand R., Ledoux C., 2002, MNRAS, 332, 383

Pettini M., Smith L.J., King D.L., Hunstead R.W., 1997, ApJ, 486, 665

Pettini M., Ellison S.L., Steidel C.C., Bowen D.V., 1999, ApJ, 510, 576

Prochaska J.X., Wolfe A.M., 1999, ApJS, 121, 369

Prochaska J.X., Wolfe A.M., 2002, ApJ, 566, 68

Prochaska J.X. et al., 2001, ApJS, 137, 21

Richter P., Sembach K.R., Wakker B.P., Savage B.D., 2001, ApJ, 562, L181

Russell S.C., Dopita M.A., 1992, ApJ, 384, 508

Savage B.D., Sembach K.R., 1996, ARA&A, 34, 279

Savage B.D., Drake J.F., Budich W., Bohlin R.C., 1977, ApJ, 216, 291

Schaye J., 2001, ApJ, 562, L95

Schectman R.M., Povolny H.S., Curtis L.J., 1998, ApJ, 504, 921

Spitzer L., Jr, Fitzpatrick E.L., 1993, ApJ, 409, 299

Srianand R., Petitjean P., 1998, A&A, 335, 33

Srianand R., Petitjean P., 2001, A&A, 373, 816

Srianand R., Petitjean P., Ledoux C., 2000, Nat, 408, 931

Tumlinson J. et al., 2002, ApJ, 566, 857

Vladilo G., 1998, ApJ, 493, 583

Welty D.E., Hobbs L.M., Lauroesch J.T., Morton D.C., Spitzer L., York D.J., 1999, ApJS, 124, 465

Wiese W.L., Fuhr J.R., Deters T.M., 1996, J. Phys. Chem. Ref. Data, Monograph No. 7

Wiese L.M., Fedchak J.A., Lawler J.E., 2001, ApJ, 547, 1178

This paper has been typeset from a TEX/LATEX file prepared by the author.